Deformable acetabular cups

A biomechanical proof of concept

Joëll Magré

January 2020

Deformable acetabular cups

A biomechanical proof of concept

by

J. Magré

In partial fulfillment of the requirements for the degree of

Master of Science
in Biomedical Engineering

Delft University of Technology
To be defended on January 30th 2020

Supervisor:	K. Willemsen, MD
Thesis committee:	Prof. Dr. Ir. H.H. Weinans
	Prof. Dr. Ir. P. Breedveld
	Ir. H.M.A. Kolken

Preface

This graduation project is part of a larger research project, focusing on developing the smart implant of the future. The research project Prosperos (Printing Personalized Orthopaedic Implants) is a collaboration between several universities and companies in the Netherlands and Belgium.

After my internship at the UMC Utrecht I started my thesis on deformable acetabular cups. An exciting project I thoroughly enjoyed working on. Next to my graduation project I had the opportunity to work on several clinical 3D cases. I would like to thank Harrie Weinans for the opportunity to do my internship and thesis at the UMC Utrecht. Koen, thank you for being my supervisor during my time at the UMC Utrecht. I enjoyed working with you on the clinical 3D cases.

Thanks to Aritz Fontecha from 3D Systems for manufacturing all samples and acetabular cups and to Bart from the MTKF for assisting me in the workshop. I would like to thank Bart van der Wal and Charles Vogely for their clinical input and enthusiasm.

During this project we had regular meetings with everyone working on this project. Thank you, Amir Zadpoor, Eline Kolken, Lennart Scheys, Alexander Meynen and Christa de Jonge for all the constructive meetings.

At last I would like to thank all my friends and family for their support during my studies. The experiences I have gained during the past years are a great foundation for the future.

Abstract

Introduction   The management of large acetabular defects remains one of the most challenging aspects of revision total hip arthroplasties. Failure of frequently used acetabular reconstruction components are, among others, caused by the lack of biological fixation, a non-physiological stress distribution and stress-shielding. Attempting to diminish these drawbacks of current implants a new acetabular cup with a plastically deformable layer has been explored. The plastically deformable layer of this new acetabular cup deforms during insertion and completely fills the acetabular defect. According to Wolff's law this should reduce stress shielding and stimulate bone ingrowth.

Methods   Part one of this study explores the relationship between unit cell size and mechanical properties for the body centred cubic unit cell. Three graded lattices using different unit cell sizes were designed and 3D-printed out of commercially pure titanium (Grade 1) using selective laser melting. An unconfined compression test with cylindrical samples as well as a confined compression test with hemispherical samples were performed to obtain mechanical properties as well as assessing deformation of the lattice structures. An additional finite element study was used to validate deformation observed in the confined compression test. In part two the 4x4x4 mm unit cell size was chosen to be implemented as deformable layer for the deformable cups. Acetabular defects were made in five Sawbones hemipelves which served as the basis for the design of the 'patient specific' acetabular cups. Three triflange and two unflanged acetabular cups were designed and 3D-printed out of commercially pure titanium (Grade 1) using selective laser melting.

Results   Mechanical properties were obtained from the unconfined compression tests. Elastic moduli and yield strengths as low as 0.026 MPa and 0.076 MPa respectively were found. All acetabular cups were inserted by two orthopaedic surgeons at the UMC Utrecht. Some loose struts were observed after insertion. Segmented CT scans revealed deformation after insertion of the implants when registered onto their original CAD (Computer Aided Design) files. Cyclic testing was performed up to 1000 cycles to assess femoral head penetration under load after insertion. Additional penetration of the femoral head was found to be between 0.1781 and 0.3793 mm.

Conclusion   The concept of a deformable acetabular cups showed promising results in this study. Future work is needed to prevent strut breakage upon insertion. Also, more research is needed in the fatigue behaviour of these highly porous lattices and their biological effect on living bone tissue.

Graphical abstract

Part one

Part two

Contents

1
Introduction

The increasing number of primary total hip arthroplasties has led to an increasing number of revision total hip arthroplasties.[1] The main reason for revision surgery is aseptic loosening of the acetabular component.[2,3] The better the fixation of the component, the longer it will last without revision.

Long term fixation of the acetabular cup relies on bony ingrowth, which on its turn relies on initial stability after implantation. Regular hemispherical acetabular cups have a high chance of failure when initial stability cannot be obtained due to large acetabular bone defects.[4] Micromotion at the bone-implant interface may result in fibrous tissue formation instead of bone ingrowth, preventing biological fixation.[5,6] Biological fixation of a non-cemented hemispherical cup is unlikely when acetabular bone loss exceeds 50%.[7,8] One of the most challenging aspects of revision total hip arthroplasty is the management of large acetabular defects.[9]

The Paprosky acetabular defect classification system is often used for describing acetabular defects. The Paprosky type 3A and type 3B are considered large acetabular defects. For type 3A defects acetabular bone loss is usual present from 10 to 2 o'clock if the acetabulum is imagined as a watch face. For type 3B defects this is usually from 9 to 5 o'clock.[10]

Multiple off the shelf treatment options are available for revision total hip arthroplasty of the acetabular component, including structural allografts, non-cemented hemispherical cups, oblong cups, jumbo cups, antiprotrusio cages and Trabecular Metal augments and shells.[11–15] For large acetabular defects surgeons can also opt for a custom-made triflange acetabular implant.[16] These custom-made implants have flanges fixated with screws directed towards the ischium, pubis and ilium. However, many of these procedures are associated with high revision rates due to loosening of the acetabular cup or implant migration.[17] Due to the large bone defects not all implants will be biologically fixated.

The screwed flanges on the custom-made triflange implants generate initial stability directly after implantation. However, these flanges generate a non-physiological stress distribution within the pelvis. The screwed flanges are stiffer than the bone it is connected to. With the implant distributing the load in a non-physiological way, mainly through the flanges, the trabecular bone behind the implant becomes unloaded. This effect is known as stress-shielding.[18–20] According to Wolff's bone remodels itself when mechanically loaded. A lack of mechanical stimulus will eventually lead to bone resorbtion.[21,22]

These drawbacks of current procedures inspired us to develop a new acetabular cup which distributes stresses in a more physiological way, resulting in less stress-shielding. Current advancements in additive manufacturing, including SLM (selective laser melting) allow us to produce highly porous lattice structures.[23] The goal is to use these highly porous lattice structures to develop a deformable acetabular cup for large acetabular bone defects.

The deformable highly porous lattice structure of the implant will plastically deform and precisely fit into the acetabular cavity. Great host bone coverage should provide initial stability of the cup, the porosity allows bone ingrowth for biological fixation. Since the implant fully covers the acetabular cavity the implant actually transfers load into the acetabular cavity rather than via the flanges only. This load transfer mechanically stimulates the bone, resulting in bone ingrowth and reduction of stress shielding by the implant.

Previous research on porous structures (unpublished work by Groenewoud *et al.*) has demonstrated that these lattice structures show desirable mechanical properties which are a low elastic modulus (9.15 MPa) and large plastic deformations (61%).[24] Research into different unit cells (unpublished work by de Jonge *et al.*) demonstrated that the body centred cubic (BCC) unit cell was consistently the least stiff unit cell. This is a desirable property when designing plastically deformable implants. However, when mechanically testing highly porous hemispherical acetabular cups the push in forces were very high (3.33 kN to 14.8 kN).[25] These forces were considered to be too high for complex acetabular revision surgery, especially when the medial wall of the acetabulum is weak. Therefore, the push in force at which the scaffold deforms should be lowered.

This thesis is divided into two main parts. Part one consists of experimental tests to obtain mechanical properties of highly porous BCC (body centred cubic) lattice structures. Both the deformation in an unconfined and confined environment will be assessed. The deformation in a confined environment will also be evaluated using finite element modelling.

Part two is more focused on the clinical implication. Five porous deformable cups are designed and inserted into a Sawbones pelvis by two orthopaedic surgeons. These cups will be cyclically tested, simulating a walking motion, to assess additional penetration of the femoral head after insertion.

2
Part one

2.1 Introduction

Understanding material properties of lattice structures is important when designing plastically deformable acetabular cups. Since the deformable acetabular cup in previous experiments was rendered to be too stiff, the porous structure needs to be re-designed to obtain a lower elastic modulus and a lower yield strength. A couple of parameters can be adjusted to obtain these properties. Since the material of choice is commercially pure titanium (CP-Ti grade 1) for its ductile behaviour, other parameters have to be altered.[26] Strut thickness is currently limited to 200 μm, which is also the minimal thickness used in the previously printed deformable acetabular cups (unpublished work by de Jonge *et al.*).[25] Strut length can be increased by upsizing the unit cell.

The goal of these mechanical tests is defining the mechanical properties of porously graded lattice structures constructed out of body centred cubic unit cells. It is expected that the elastic modulus and the yield strength greatly decreas with increasing strut length. The relationship between the increasing unit cell size and decreasing elastic modulus will also be looked into.

The BCC unit cell is characterized by its low compressive strength, as well as its space filling capacities (lateral expansion) as described in both previous experiments and literature.[25,27] The unit cell is therefore suited for the design of intentionally compliant structures. This part consists of two experiments and a finite element validation. In the first experiment cylindrical samples are used to assess the mechanical properties of lattice structures (BCC unit cell) with larger unit cell sizes. In the second experiment hemispherical samples and a mould are used to assess the behaviour of the lattice structure when pressed into a confined space. Since the deformability of the lattice structure seems to be reliable on the large lateral expansion of the structure the question is how the lattice structure behaves when pushed into a confined space. The confined compression test is simulated in a finite element analysis to asses internal deformability and stress distribution.

2.2 Materials and methods

2.2.1 Lattice structure design

Lattice structures are porous structures consisting of unit cells. Unit cells are the individual building blocks that eventually form the lattice structure. The unit cell used in these experiments is the body centred cubic (BCC) unit cell (Figure 1).
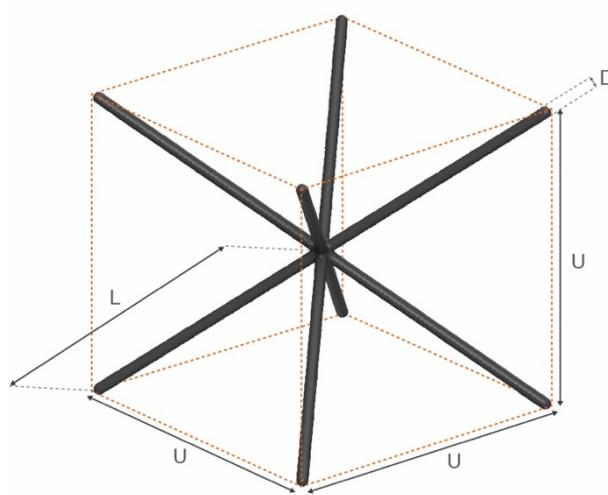
Figure 1: Design of the body centred cubic (BCC) unit cell with the representation of the strut length (L), strut diameter (D) and unit cell size (U).

The body centred cubic unit cell is isotropic, it consists of eight struts of equal length and nine nodes. The eight struts are all positioned with a 45° angle between them, all struts are connected in the centre. The size of the unit cell (U) is described by the box the unit cell fits in. The unit cell size is related to the strut length (L). The strut length can be described as a function of the unit cell size by the following equation:

$$L = \frac{\sqrt{3U^2}}{2}$$

2.2.2 Cylindrical samples

Three porous cylindrical samples were designed using the 3-Matic Medical software package (Version 13, Materialise, Belgium). The samples were 81 mm in height and had a diameter of 40 mm. The BCC unit cell was used to create the porous scaffold. Three types of samples were designed, each with a different unit cell size. The infill with the BCC unit cells done via a direct patterning approach.[28] The cylinders are divided into three equal sections with each a different strut thickness to create a gradual porosity (Figure 2). This porosity gradient is chosen because the final implant will most likely also feature a porosity gradient transitioning from the solid cup to the most porous outer layer.
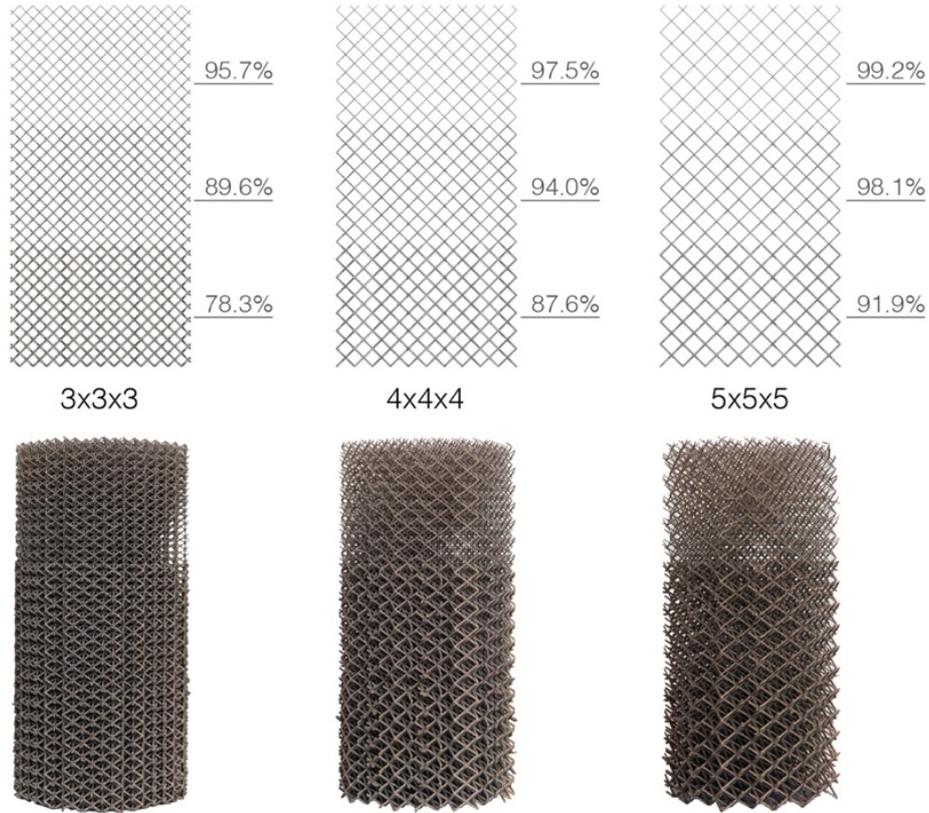
Figure 2: Design of the porously graded cylinders. Unit cell size; left: 3x3x3 mm, middle: 4x4x4 mm, right: 5x5x5 mm. The porosity gradient is obtained by adjusting the strut thickness; in all samples from top to bottom: 0.20 mm, 0.31mm and 0.45 strut thickness.

The theoretical densities of the sections are defined as the ratio between the volume of the lattice ($V_{Lattice}$) structures (out of CAD) and the volume of a solid section (V_{Solid}). The theoretical density can be described by the following equation:

$$Theoretical\ density\ [\%] = \frac{V_{Lattice}}{V_{Solid}} \cdot 100$$

The theoretical porosity can subsequently be expressed as:

$$Theoretical\ porosity\ [\%] = 100 - Theoretical\ density$$

The properties of the samples are displayed in Table 1.

Table 1: Properties of cylindrical samples

	Unit cell size [mm]	Strut diameter [mm]	Strut length [mm]	Theoretical density	Theoretical porosity
	3x3x3	0.45	2.598	21.7 %	78.3 %
Sample 1	3x3x3	0.31	2.598	10.4 %	89.6 %
	3x3x3	0.20	2.598	4.3 %	95.7 %
	4x4x4	0.45	3.464	12.4 %	87.6 %
Sample 2	4x4x4	0.31	3.464	6.0 %	94.0 %
	4x4x4	0.20	3.464	2.5 %	97.5 %
	5x5x5	0.45	4.330	8.1 %	91.9 %
Sample 3	5x5x5	0.31	4.330	1.9 %	98.1 %
	5x5x5	0.20	4.330	0.8 %	99.2 %

2.2.3 Hemispherical samples and mould

Three porous samples were designed using the 3-Matic Medical software package (Version 13, Materialise, Belgium). These samples were also lattice structures using the BCC unit cell and a direct patterning approach.[28] The three sample types all featured, as in the previous experiment, different unit cell sizes. These samples do also have a porous gradient obtained by different strut thickness. The design and dimensions of the samples can be seen in Figure 3. The porosity values, strut thicknesses and strut lengths are the similar to the values of the cylindrical samples. Only these samples have a two-layer gradient using the 0.20 mm and 0.31 mm strut thickness. These properties are shown in Table 1.
A mould was milled out of a solid block of aluminium by the MTKF (Medische Technologie & Klinische Fysica) at the UMC Utrecht. The mould with its dimensions is shown in Figure 3.
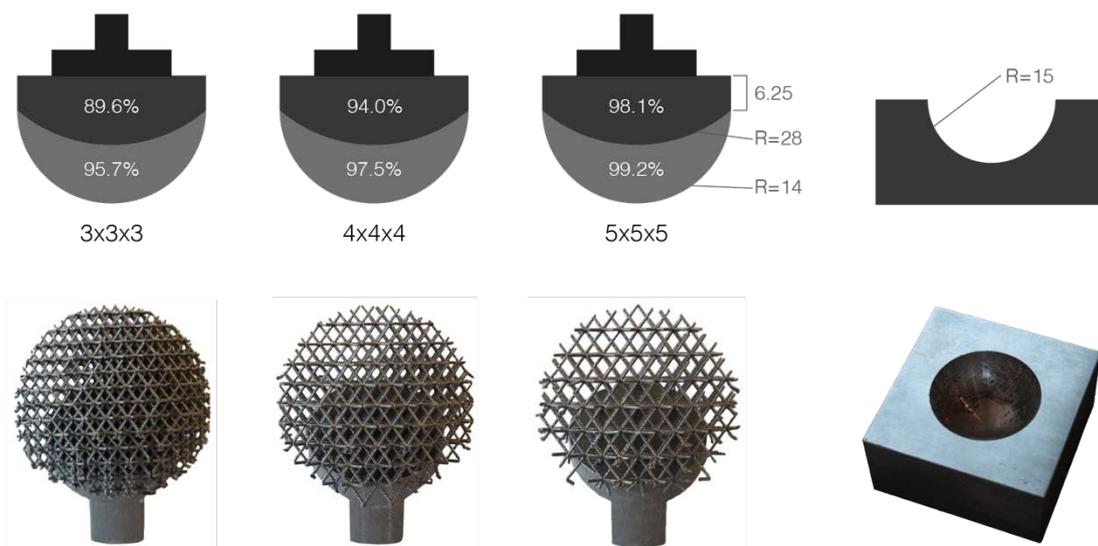
Figure 3: Design parameters of the hemispherical samples and aluminium mould (top). Photographs of the manufactured hemispherical samples and aluminium mould(bottom).

2.2.4 Material and production

Due to its high strength to weight ratio Ti6Al4V is an often-used material for load-bearing orthopaedic implants. Although Ti6Al4V remains the strongest material for statically loaded applications, the non-alloyed material; commercially pure titanium (CP-Ti), shows mechanical behaviour similar to tantalum.[26] CP-Ti outperforms Ti6Al4V in terms of high cycle fatigue strength and could therefore be more suitable for cyclically loaded implants such as acetabular components in hip arthroplasties.[26]

The goal of this study is to make highly deformable structures to design deformable acetabular implants. The ductile behaviour of CP-Ti makes this the material of choice for the production of porous deformable lattice structures and acetabular implants. The bulk properties of CP-Ti and Ti6Al4V are shown in Table 2.[29,30]

All samples were manufactured by 3D Systems (Leuven, Belgium) using selective laser melting (SLM). For these samples the ProX DMP 320 (3D Systems, Leuven, Belgium) SLM machine was used.[31] The material used to produce the samples is commercially pure titanium (Grade 1) in powder form.[29] The parts are build up layer by layer by laser scanning a powder bed. The laser melts the titanium powder which binds together. A new layer of titanium powder is then placed onto the powder bed and the laser scans the powder bed again, binding the powder. This layer by layer process eventually forms the part.[32,33] Strut thickness of the lattice structure is currently limited to 200 µm.
Each sample type was produced three times resulting in a total of nine samples per experiment.

Table 2: Mechanical properties of CP-Ti (Grade 1) and Ti6Al4V (Grade 5). CP-Ti has an elastic modulus similar to Ti6Al4V but a yield strength almost three times as low.

	CP-Ti (Grade 1)	Ti6Al4V (Grade 5)
Density [g/cm^3]	4.51	4.42
Young's modulus [GPa]	105-120	105-120
Ultimate strength [MPa]	500 ±30	1180 ±30
Yield strength [MPa]	380 ±30	1090 ±30
Elongation at break [%]		
Horizontal direction – XY	29 ±5	9 ±2
Vertical direction - Z	30 ±5	9 ±2

2.2.5 Mechanical testing

All samples were subjected to a static compression test on a Lloyd LS 5 universal test machine (Amatek, Berwyn, United States) with a 5 kN load cell. The cylindrical samples were placed in between compression plates, the hemispherical samples were placed into an upper vice grip while the mould was placed on the lower compression plate (Figure 4). All cylindrical samples were subsequently compressed with a compression rate of 2 mm/min up to a force of 5 kN. All nine cylindrical samples were tested in the same manner and a video recording was made of the compression of each sample type.

The hemispherical samples were also compressed with a rate of 2 mm/min. These samples were compressed until a machine extension of 10 mm was reached. This was to make sure the solid part of the sample did not touch the mould.

The direct results from the static compression test are force-displacement curves. This data is used to obtain stress-strain curves for the cylindrical samples. The stress (σ) is calculated by dividing the applied force by the initial cross-sectional area. The strain (ε) is defined as the displacement divided by the original sample height. The elastic moduli were calculated from the slope of the stress-strain curves in the linear elastic regions of the cylindrical samples using the following formula:

$$E = \frac{\sigma}{\varepsilon}$$

The compressive yield strengths were determined from the stress-strain curves of the cylindrical samples using the 0.2% offset method.

It is important to understand that the material properties described in these experiments describe a different concept when concerning highly porous lattice structures. When referring to solid materials the material properties describe the intrinsic properties of the material, when referring to highly porous lattice structures it describes the macroscopic properties of the structure.[34]
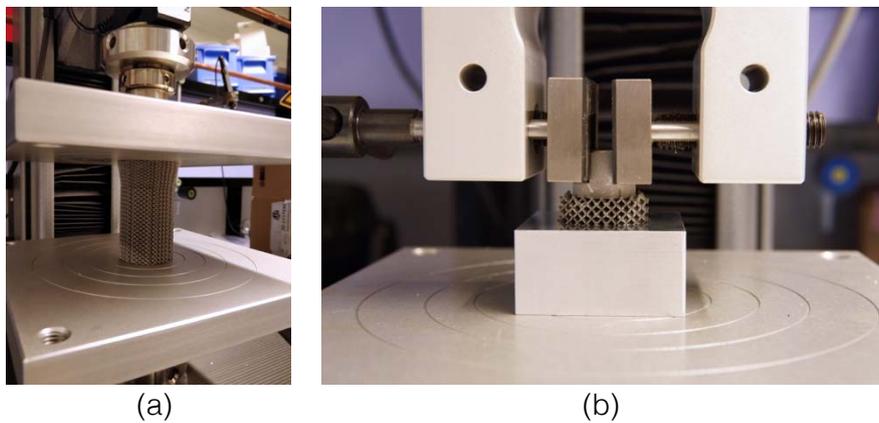
Figure 4: Test setup of the compression tests; cylindrical samples (a), hemispherical samples (b).

2.2.6 Finite element analysis

A simplified two-dimensional FEM (finite element method) model was created in Abaqus (Version 6.14, Dassault Systemes, France) to assess stress distribution and deformation of the hemispherical samples. The cross sections of the porous sections of the hemispherical samples were created in Abaqus together with a discrete rigid press (representing the solid part of the sample) and a discrete rigid mould.

For simplification the porous part of the sample was modelled as a solid using the material properties found in the compression test with cylindrical samples. The average elastic modulus found in the first experiment (Table 3) and a Poisson's ratio of 0.48 was used to define the elastic material behaviour. For isotropic solid materials the theoretical Poisson's ration cannot exceed 0.5. However, experiments have shown that highly porous lattice structures, including the BCC unit cell, can show atypical behaviour and have a Poisson's ratio higher than 0.5.[25] A Poisson's ratio higher than 0.5 is an invalid input in Abaqus so a high Poisson's ration of 0.48 was chosen to avoid computational errors. The plastic material behaviour was described by fitting a polynomial through the plastic region of the data points. This data was used to describe the plastic material behaviour. The Abaqus model and the data of one of the plastic regions (4x4x4 mm unit cell size, 0.2 mm strut thickness) can be seen in Figure 5. The

elastic and plastic data of all samples and strut thicknesses can be found in appendix Figure A 1-Figure A 4. Density was calculated by using the theoretical density values shown in Table 1 as a percentage of the bulk property density value shown in Table 2.

A displacement of 7 mm was exerted on the samples (Abaqus) to validate the stress distribution and deformation within the printed titanium samples.
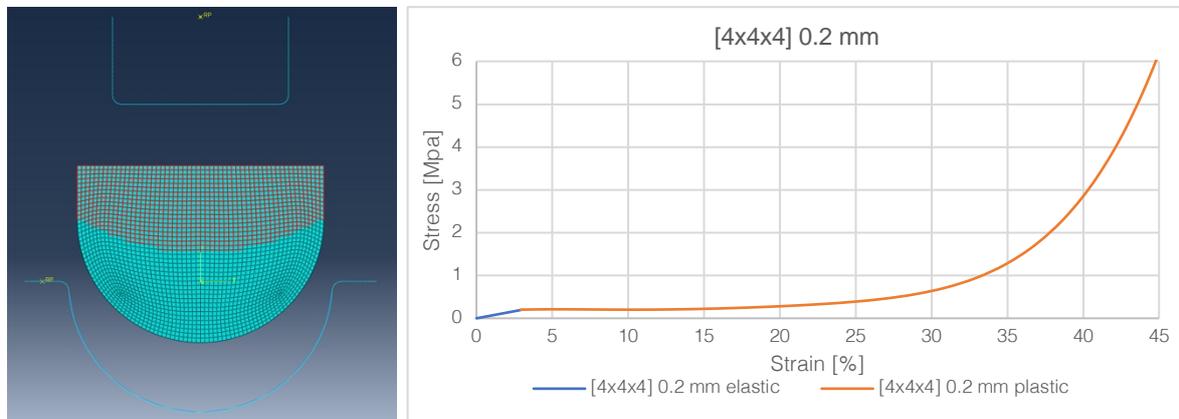
Figure 5: Left: mesh of the samples used in Abaqus for the finite element method. The red coloured elements are the inner struts with a thickness of 0.31 mm, the other elements are the outer more porous struts with a thickness of 0.2 mm. On the right the elastic and plastic data extracted from the cylindrical sample compression test of the 4x4x4 mm sample with a 0.2 mm strut thickness.

2.3 Results

2.3.1 Cylindrical samples

All nine cylindrical samples were compressed until a force of 5 kN was reached. The resulting force-displacement curves were converted into stress-strain curves. The smaller unit cell size samples (3x3x3 mm) results in a stiffer and stronger structure than the larger unit cell size samples (5x5x5 mm). The stress-strain curves of the static compression test can be seen in Figure 6. The three linear elastic sections with different porosities can clearly be differentiated in the 4x4x4 mm and 5x5x5 mm unit cell size samples. In these plots the three plateau regions are clearly visible. The stress-strain curves of the 3x3x3 mm unit cell size does not show three, but two linear elastic sections indicating the least porous section (0.45 mm strut thickness) did not deform under a 5 kN load. This is further illustrated in Figure 7.

Figure 7 shows the compression of all sample types at corresponding time intervals. At the latest time interval the compression force is 5 kN and it can be seen that the less porous sample (3x3x3 mm) has deformed considerably less than the more porous samples, as can also be seen from the stress-strain curve (Figure 6).
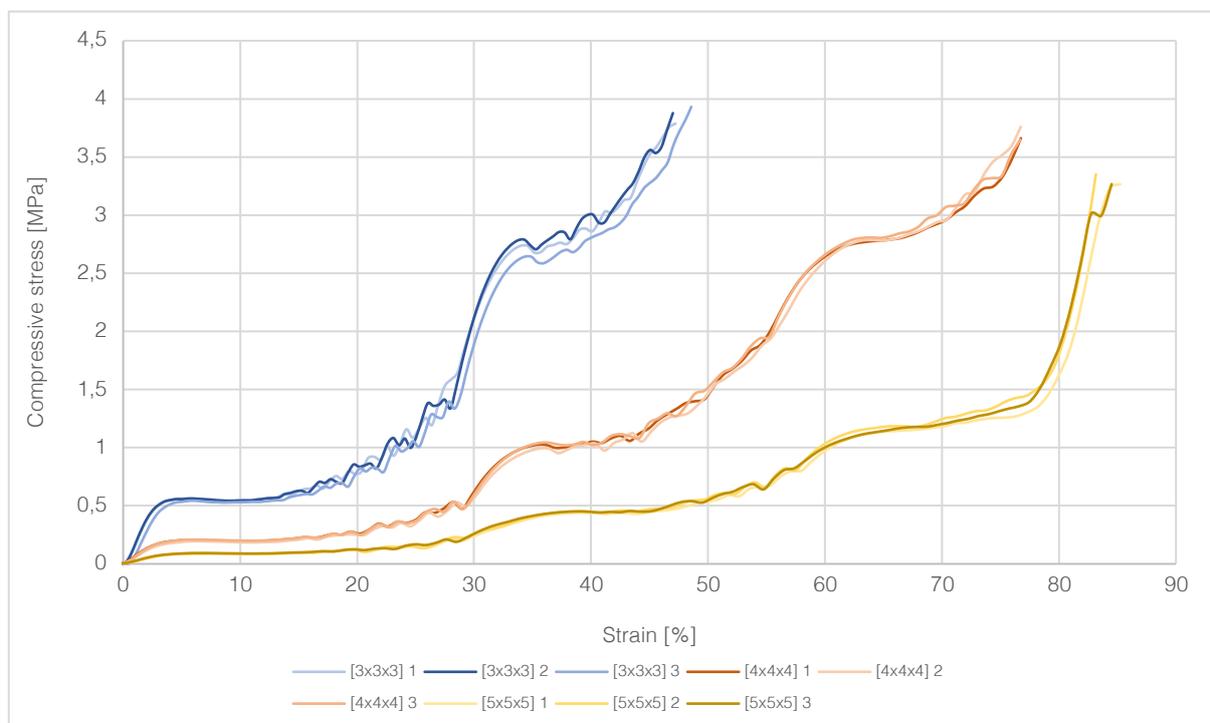
Figure 6: Stress-strain curves of the compression test of the cylindrical samples. Each sample type was produced three times, hence the three lines that are grouped. The 3x3x3 mm samples are displayed in blue, the 4x4x4 mm samples in orange and the 5x5x5 mm samples in yellow.

All samples show ductile behaviour characterized by the plateau region in the plastic region. The elastic moduli found and compressive yield strengths for each porous section of the samples are show in Table 3. The elastic modulus and compressive yield strength could not be determined for the 0.45 mm strut thickness section (3x3x3 mm sample) because the 5 kN compression force did not deform this section.
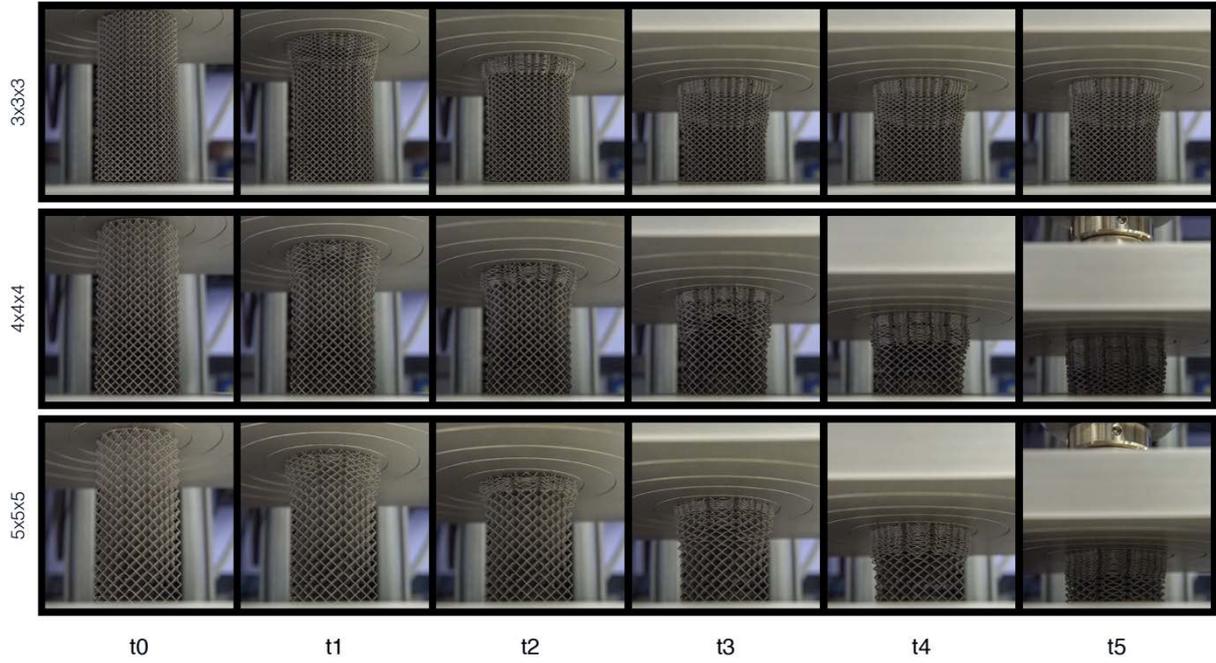
Figure 7: Compression of the cylindrical samples at different time intervals. Top: 3x3x3 mm, middle: 4x4x4 mm and bottom: 5x5x5 mm. At t5 the maximum compression force of 5 kN is reached for the 4x4x4 mm and 5x5x5 mm samples. Note that at t3 a load of 5 kN is reached for the 3x3x3 mm sample.

All samples deformed significantly during compression, the largest unit cell size (5x5x5 mm) deformed the most. The height of the 3x3x3 mm samples decreased 41.6% on average, for the 4x4x4 mm samples this was 71.1% and for the 5x5x5 mm samples 79.2%. The average lateral expansion of the samples at the fully deformed sections was 16.8% for the 3x3x3 mm samples, 16.8% for the 4x4x4 mm samples and 17% for the 5x5x5 mm samples.

Table 3: Mechanical and dimensional properties of the cylindrical samples extracted from the compression test

Unit cell size [mm]	Strut thickness [mm]	Porosity	Elastic modulus [MPa]	Compressive yield strength [MPa]
3x3x3	0.20	95.7 %	0.224 ±0.013	0.499 ±0.014
3x3x3	0.31	89.6 %	0.380 ±0.037	2.368 ±0.090
3x3x3	0.45	78.3 %	-	-
4x4x4	0.20	97.5 %	0.066 ±0.007	0.168 ±0.006
4x4x4	0.31	94.0 %	0.145 ±0.006	0.857 ±0.030
4x4x4	0.45	87.6 %	0.190 ±0.017	2.462 ±0.043
5x5x5	0.20	99.2 %	0.026 ±0.001	0.076 ±0.007
5x5x5	0.31	98.1 %	0.039 ±0.008	0.383 ±0.030
5x5x5	0.45	91.9 %	0.087 ±0.012	1.029 ±0.021

Plotting the elastic moduli against unit cell size for a given strut thickness gives a negative correlation between increasing unit cell size and the decrease of the elastic modulus (Figure 8). An exponential trend line appears to be a good fit through these data points demonstrating a negative exponential relationship between the unit cell size and the elastic modulus for the BCC unit cell.
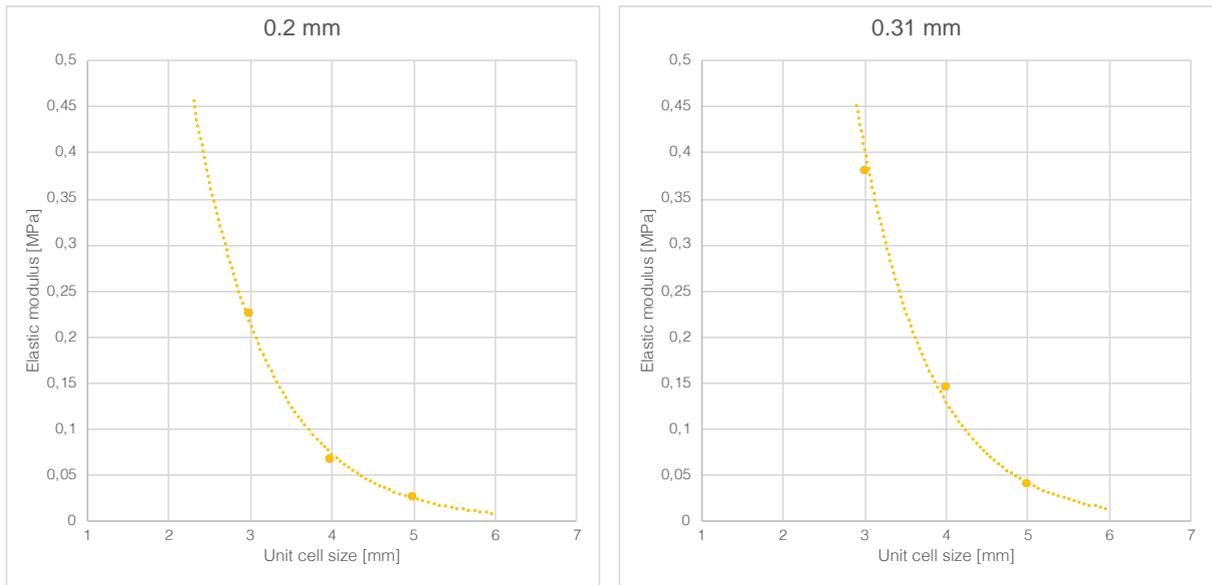
Figure 8: Unit cell size plotted against the elastic modulus demonstrating a negative exponential relationship between the unit cell size and the elastic modulus for the BCC unit cell.

2.3.2 Hemispherical samples

The hemispherical samples were compressed into the aluminium moulds until a machine extension of 10 mm was reached. The 3x3x3 mm unit cell samples required the highest push-in force to compress the samples into the mould. The machine extension is plotted against the force in Figure 9.
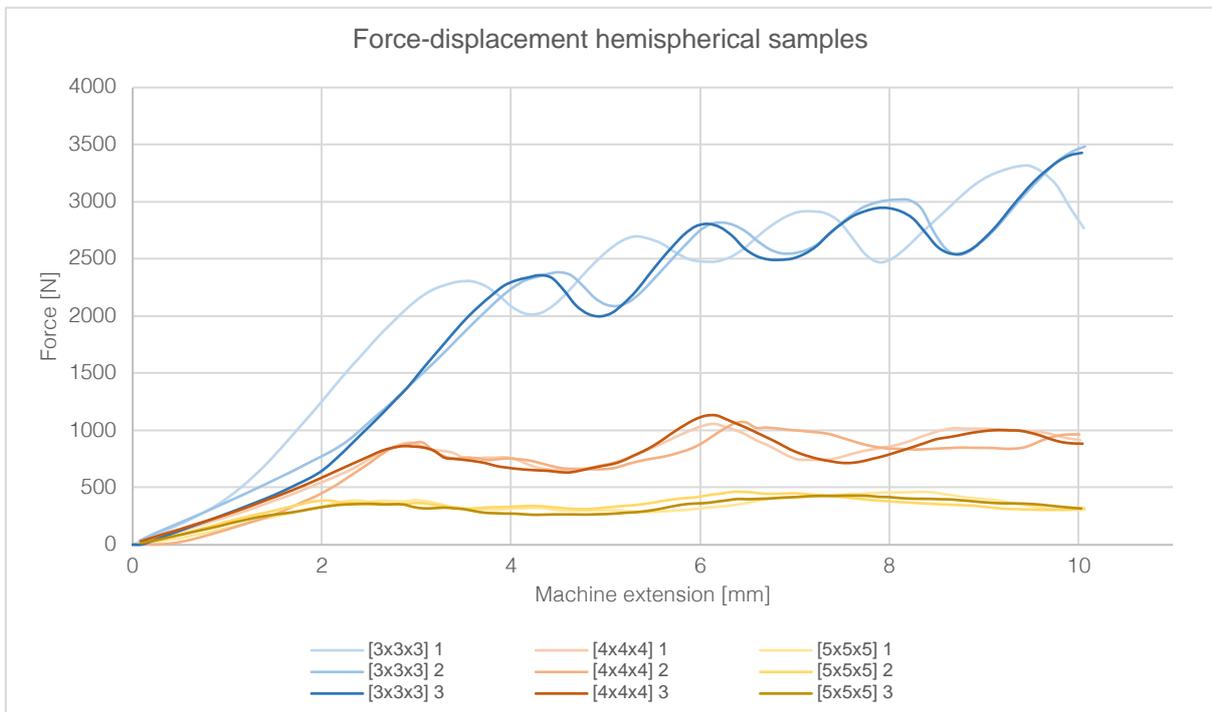
Figure 9: Force-displacement curves of the compression test of the hemispherical samples. The 3x3x3 mm samples are displayed in blue, the 4x4x4 mm samples in orange and the 5x5x5 mm samples in yellow.

When examining the samples after compression it is shows that the least porous (0.31 mm strut thickness), and thus least stiff section appears to have deformed the most. Pictures of the deformed

samples are shown in Figure 10. The outer layer of the lattice structure seems to be more or less intact, especially in the 3x3x3 mm and 4x4x4 mm unit cell size samples.
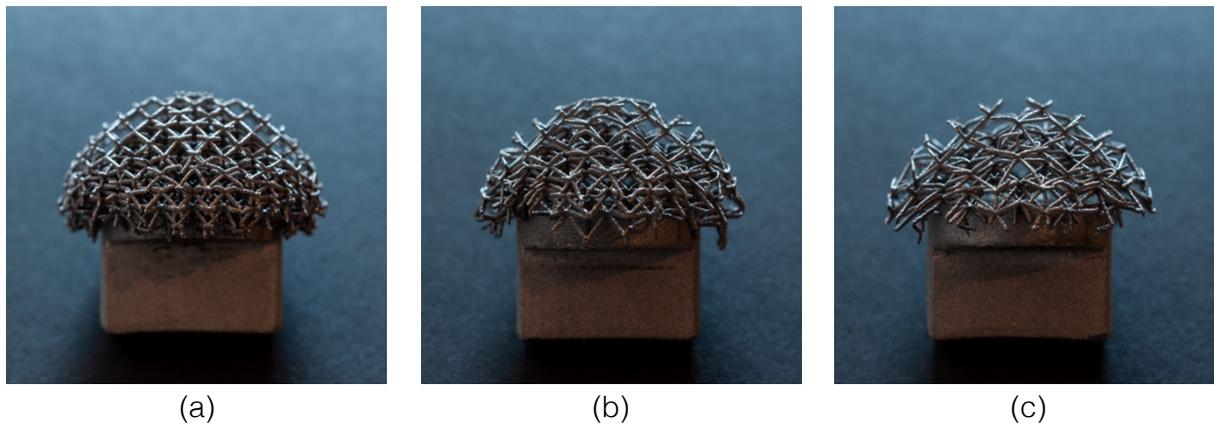
Figure 10: Hemispherical samples after compression. 3x3x3 mm unit cell size (a), 4x4x4 mm unit cell size (b) and 5x5x5 mm unit cell size (c).

2.3.3 Finite element validation

A finite element simulation was done for each hemispherical sample type to visualize the stress distribution and material displacement within the sample. A stress concentration is visible around the edges of the solid part of the sample. Higher stresses are observed in the less porous section than in the highest porous sections in all samples (Figure 11). Lower stresses are observed in the outer section (most porous section) of the samples.
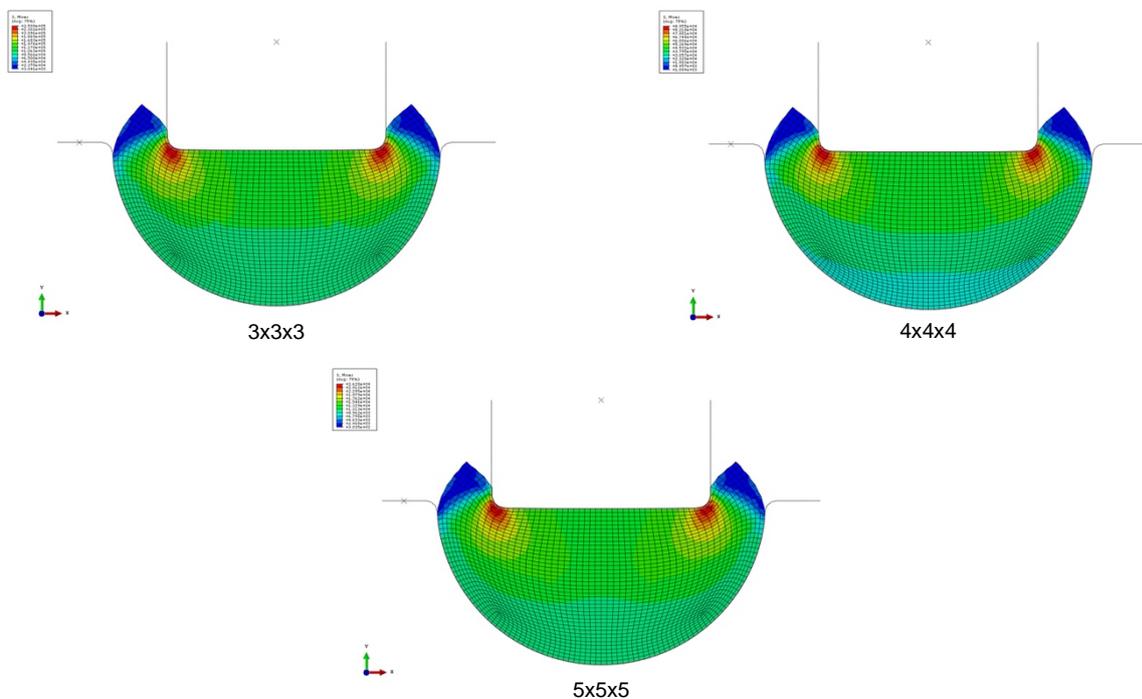
Figure 11: Stress distribution in the finite element models. Top left: 3x3x3 mm unit cell size, top right: 4x4x4 mm unit cell size, bottom: 5x5x5 mm unit cell size.

21

Consistent with the observation of the compressed hemispherical samples the finite element models show larger deformations in the less porous section of the samples than in the higher porous section. This can be seen in the compressed finite element samples in Figure 12.
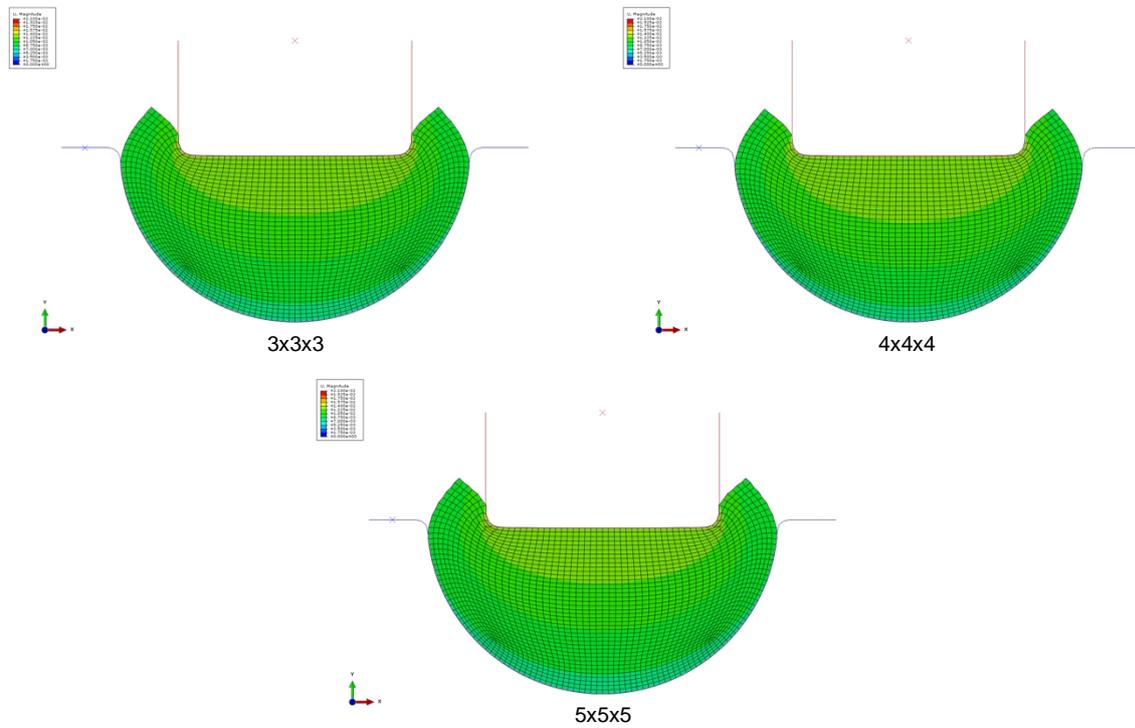
Figure 12: Deformation within the finite element models. Top left: 3x3x3 mm unit cell size, top right: 4x4x4 mm unit cell size, bottom: 5x5x5 mm unit cell size.

2.4 Discussion

The experiments were conducted to evaluate the mechanical properties and behaviour using an increasing unit cell size to optimize deformability. The body centred cubic (BCC) unit cell was evaluated since previous experiment showed this was the most compliant unit cell.[25] The first experiment with cylindrical samples was performed to obtain the mechanical properties of increasing unit cell sizes. The compression test with hemispherical samples was performed to assess deformability of the lattice structure in a confined space. This experiment was also evaluated using a simplified finite element model in Abaqus.

The stress strain curves resulting from the compression test with cylindrical samples show a linear elastic region and a plateau region as expected. The three porous sections are discernible in plots of both the 4x4x4 mm and 5x5x5 mm unit cell sizes. All samples show the same type stress-strain curves although they represent different stiffnesses and compressive strengths. However, it is apparent from the stress strain curves the samples with a higher porosity (thinner strut thicknesses or larger unit cell) show a larger plateau region in the plastic deformation phase (Figure 6). Elastic moduli and compressive yield strengths as low as 0.026 MPa and 0.076 MPa respectively were found in this experiment. The low elastic modulus and large deformation capacity of the BCC unit cell found in this study are also described in literature.[27] The stress-strain curves also show some spikes right after the plateau region, when material densification is happening. These spikes indicate the breakage of struts. After compression no loose struts came out of the samples. This indicates the struts broke at one end only, at this point the strut is no bearing part of the lattice structure anymore. The samples deformed collapsing a layer by layer.
This is consistent with the failure mechanism described in literature, manufacturing irregularities significantly affect the mechanical properties of the lattice structure.[35] The lattice structure shows heterogeneous behaviour while at strut level local strain concentrations accumulate at the weak spots, resulting in strut failure.[36]

The elastic modulus and compressive yield strength were determined from the stress-strain curves of the compression test. As shown in Figure 7 the samples showed significant lateral expansion during compression. This is a desired property when designing the acetabular cups since this lateral expansion fixates the cup in the acetabulum. This is due to geometrical properties of the BCC unit cell. The deformability of the unit cell is highly dependent on the lateral expansion. The lateral expansion means that the cross-sectional area increases during compression. When calculating the stress, the engineering stress was calculated using the original cross-sectional area of 40 mm. The true compressive stress is lower than the engineering compressive stress, this is also true for solid materials. However, the large lateral expansion of these structures might result in a significant lower true stress.
The cylindrical samples were all a graded design, this was decided because the final acetabular cup will most likely also feature a graded design to prevent stress shielding. This graded design is divided into uniform sections. The mechanical properties obtained from a graded design in which there is a gradient within the unit cell might not be exactly corresponding with the results obtained from a uniform design.[34]

Figure 8 demonstrates a negative exponential relationship between the unit cell size and the elastic modulus. Increasing the unit cell size dramatically reduced the elastic modulus of the lattice structure. Between the 3x3x3 mm unit cell size and the 5x5x5 mm unit cell size there is roughly a factor 10 difference in elastic modulus (0.224 MPa and 0.026 MPa respectively).
The exponential relationship is currently based on three unit cell sizes, to further analyse this relationship experiments with more unit cell sizes are needed.

The hemispherical samples were all compressed into an aluminium mould until a deformation of 10 mm was reached. Where the three porous sections were clearly discernible in the unconfined compression test

with cylindrical samples, this is not the case with the hemispherical samples. Where the cylindrical samples showed significant lateral expansion, this was not possible since the samples were confined by the mould. The confined space seems to stiffen the lattice structure in a way deformation happens mostly in the stiffer, les porous, section of the sample. Still the push-in forces for the hemispherical 4x4x4 mm unit cell size samples are considerably lower than the push-in forces of the 3x3x3 mm unit cell size samples.

The plateau stresses appear to be less constant for the confined compression test than for the unconfined compression test (Figure 9 and Figure 6). This is probably caused by the restriction in the lateral directions causing the BCC unit cells to collapse within the parameters of the confinement.

The finite element analysis showed larger deformations in the least porous/stiffer section of the samples. This is in line with the observations from the hemispherical samples. This finite element model is a simplification of the real samples and therefore has limitations. One of the biggest limitations is the simplification as a solid. As seen in the samples the structure deforms by collapsing layer by layer meaning there is a space filling volume reduction happening. The mechanical properties found in de unconfined cylindrical compression test were used as mechanical properties for the modelled solid, however, a reduction of volume cannot take place in a solid material. This is the reason only 7 mm of deformation was possible in the finite element model versus the 10 mm used in the real samples. Another limitation is the simplification to a two-dimensional model.

A more accurate representation can be created by modelling the entire lattice structure. Though manufacturing irregularities affect the mechanical properties of the lattice structure model based on straight trusses will not give an accurate representation. It is described in literature that these manufacturing irregularities can be implemented in finite element models.[35]

Though it is possible to create strut lengths up to 4.33 mm using SLM, some limitations were found when removing the samples from the build plate. The large strut lengths make it not possible to directly grow the scaffold on the build and are therefore printed on a solid block of titanium. The samples are removed from the solid blocks using wire EDM (Electrical Discharge Machining) method.[37] The inaccuracies of the process make it difficult to remove the structures. For the 5x5x5 mm unit cell size with its 4.33 mm strut length this resulted in damaged and open-ended struts. Therefore, the 5x5x5 mm unit cell size is considered a non-viable scaffold geometry for real production.

In these experiments, samples featuring a porosity gradient were designed and used. The final acetabular cups will feature some sort of porosity gradient. Previous experiments (unpublished work by de Jonge *et al.*) have shown that the transition between a solid titanium layer and very thin struts (0.20 mm strut thickness) might lead to strut failure at the interface.[25]

The current samples are tested as manufactured without any post processing. Post processing can further optimize mechanical properties of the lattice structures. A recommended post processing step is HIP (Hot Isostatic Pressing) treatment.[38] For CP-Ti HIP treatment will further reduce the yield strength of the bulk material and increase ductility.[29] In theory this should mean greater deformability and less strut breakage in the lattice structures.

2.5 Conclusion

Increasing the unit cell size considerably reduces the elastic modulus and compressive yield strength of lattice structures constructed out of the body centred cubic (BCC) unit cell. This experiment shows a relationship that is negatively exponential.

The large deformability of the BCC unit cell is desirable for designing deforming acetabular cups. However, it was observed that in a confined space the lattice structure becomes stiffer. In the graded design the least porous (stiffest) section deformed the most. This was also observed in a finite element validation where also most deformation took place in the least porous section. Also, the highest stresses within the material were in the least porous section.

For the design of the acetabular cups the 4x4x4 mm body centred cubic unit cell will be used. For now, the 5x5x5 mm unit cell size is not a viable option for production. The 3x3x3 mm unit cell size has an elastic modulus more than three times higher than the elastic modulus of the 4x4x4 mm unit cell size. The push-in forces required to deform the 3x3x3 mm lattice structure were considered too high for complex acetabular revision surgery in previous experiments.

The deformable parts on the acetabular cups will be filling a solid volume using a direct patterning approach. In terms of geometry retainment, the 4x4x4 mm unit cell size is also more favourable as opposed to the larger 5x5x5 mm unit cell size.

3

Part two

3.1 Introduction

In part one the mechanical properties of BCC unit cell lattice structures were obtained. The 4x4x4 mm unit cell size was chosen to be used for the deformable part of the implants. The goal of part two is implementing the knowledge gained in previous experiments in designing plastically deformable acetabular cups for large acetabular defects.

One of the most important aspects of the deformable acetabular cup is that the deformable part deforms during insertion. The challenging aspect is that no additional deformation occurs when the implant is under load, during walking for example. These aspects of the deformable acetabular cup will be investigated in this second part.

Acetabular defects are made in five Sawbones hemipelves which will be the basis for the acetabular cups. Five acetabular cups featuring deformable layers are designed for the corresponding hemipelves. All acetabular cups are inserted into their corresponding hemipelves by two orthopaedic surgeons at the UMC Utrecht. After insertion the hemipelves with acetabular cups are cyclically tested to assess additional penetration of the femoral head, which could be an indication of additional deformation.

3.2 Material and methods

3.2.1 Sawbones

Five Sawbones biomechanical composite hemipelves (right side) were ordered from Sawbones Sweden. Sawbones biomechanical bones are a validated alternative to cadaveric bones.[39,40] The used composite hemipelves consist of a 10 PCF solid foam inner core simulating trabecular bone and a short fibre filled epoxy as simulated cortical bone.[41] The mechanical properties of the 10 PCF solid foam and short fibre epoxy as well as the mechanical properties of human bone are shown in Table 4 Mechanical properties of the Sawbones hemipelves are from the Sawbones data sheet.[41] The properties of the human bone are based on literature.[42–45]

Table 4: Mechanical properties of the Sawbones hemipelvis and the human pelvic bone.

	Sawbones		Human pelvic bone	
	10 PCF solid foam	*Short fibre epoxy*	*Trabecular bone*	*Cortical bone*
Elastic modulus (compression) [MPa]	58	16.700	49.7 - 96	18.600
Yield strength (compression) [MPa]	2.2	157	0.22 – 0.64	161 - 183

In all five hemipelves acetabular defects were made according to the Paprosky acetabular defect classification system.[10,46] In two hemipelves a Paprosky type 3A defect was created and type 3B defects were created in the other three hemipelves.

After the defects were made a CT-scan was made of all hemipelves using a 0.8 mm slice thickness (Philips IQon Spectral CT, UMC Utrecht). The DICOM files of the scans were segmented using the Mimics Medical software package (Version 24, Materialise, Leuven, Belgium) to create three-dimensional computer models. The rendered images of the created Paprosky type 3A and 3B defect are shown in Figure 13.

<div align="center">(a)   (b)</div>
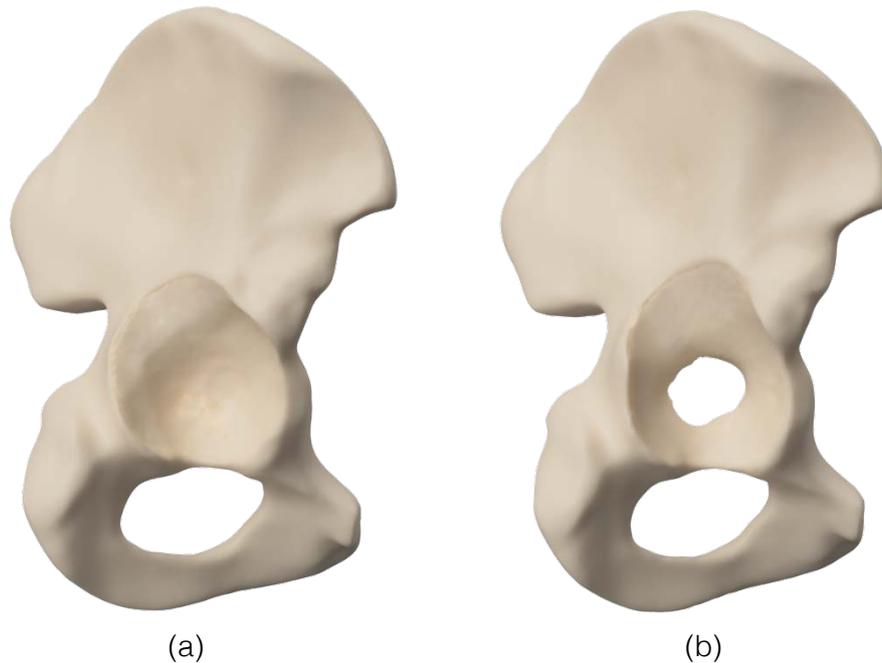
Figure 13: Rendered images of the acetabular defects created in the Sawbones hemipelves. Paprosky type 3A (a), Paprosky type 3B (b).

3.2.2 Implant design

Using the CAD (Computer Aided Design) models of the Sawbones hemipelves five 'patient specific' acetabular cups were designed using the 3-Matic software package.

To determine the correct position of the acetabular cup without the contralateral hemipelvis (left side) present, the hemipelvis was mirrored around the articular surface of the pubis. A fitting sphere was fitted in the acetabular cavity to determine the centre of rotation. Using this centre of rotation, a 44 mm hemispherical acetabular cup designed in SolidWorks (version 2017, Dassault Systemes, France) was imported and placed at 55° inclination and 20° anteversion.[47]

Five different acetabular cups were designed, these cups can be divided into two major concepts; acetabular cups without flanges and acetabular cups with flanges. The cups with flanges feature two design concepts, a version with the deformable outer layer attached and an undersized version that requires a separate deformable mesh. The porous layers of the cups are constructed out of BCC unit cells using a direct patterning approach.[28] The lattice structure is oriented in the direction of insertion, favourable to the direction of lateral expansion of the BCC unit cell. The specifications of the acetabular cups are shown in Table 5.

The three oversized cups with attached deformable layer have a graded porosity. They consist of a porous non-deformable section with a strut thickness of 0.5 mm and a deformable outer layer with a strut thickness of 0.2 mm. The cups are 4 mm oversized in the direction of insertion. The deformable layer has a thickness of 8 mm. One of the oversized cup features three flanges directed towards the

ischium, pubic and ilium. The solid part of the cups without flanges is designed to lay flush with the cortical shell of the Sawbones hemipelves.

The two undersized cups are 6 mm undersized and require the 10 mm generic mesh. Both these cups feature three flanges directed towards the ischium, pubis and ilium. SB2 has a smaller unit cell size which is more comparable to the currently available aMace cups.[48] The SB4 cup has a slightly larger 2.5x2.5x2.5 mm unit cell size. The strut thickness of the non-deformable porous sections is 0.3 mm. Undercuts were removed of all implants to ensure a proper fit. The design of the five acetabular cups is shown in Figure 14.

Five 28 mm liners were produced using SLS (Selective Laser Sintering) out of PA12 (Oceanz, Ede, Netherlands).

Two types of generic deformable meshes were designed in SolidWorks (version 2017, Dassault Systemes, France). A circular mesh and an elongated mesh, both with cut-outs to improve deformability (Figure 14). The elongated part of the mesh could for instance fill the defect in the direction of the ilium. The meshes are 10 mm thick and are constructed out of the 4x4x4 mm BCC unit cell using direct patterning.[28] Both mesh types were produced in three diameter sizes; 53 mm, 63 mm and 73 mm. The designs of the deformable meshes are shown in Figure 14.

Table 5: Properties of the designed acetabular cups

Acetabular cup	Type	Defect type	Flanged/no flanges	Unit cell size [mm]
SB1	Oversized	Paprosky 3A	No flanges	4x4x4
SB2	Undersized	Paprosky 3A	Flanged	1.5x1.5x1.5
SB3	Oversized	Paprosky 3B	No flanges	4x4x4
SB4	Undersized	Paprosky 3B	Flanged	2.5x2.5x2.5
SB5	Oversized	Paprosky 3B	Flanged	4x4x4

(a)
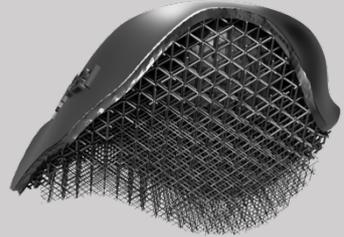
(b)
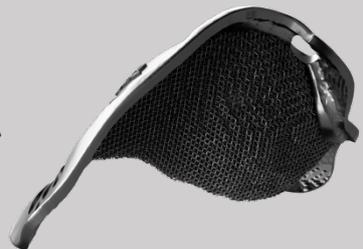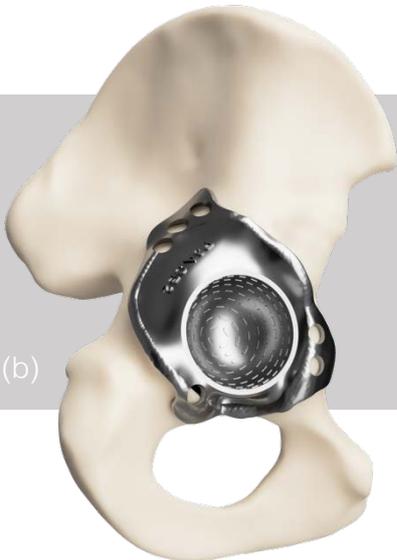
(c)
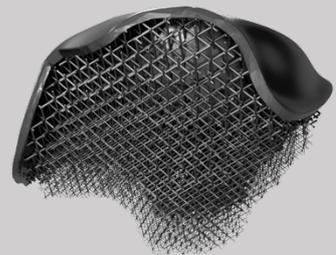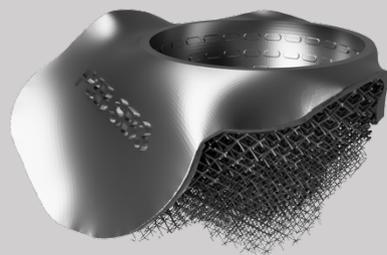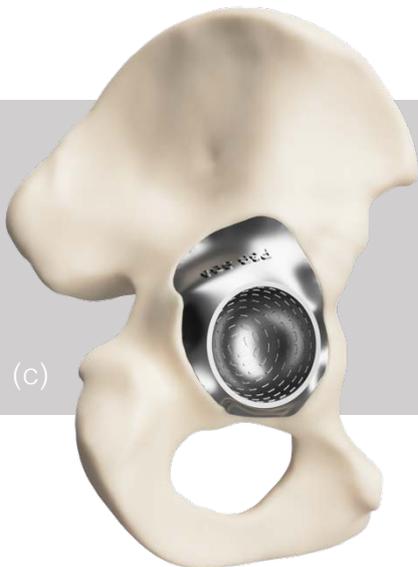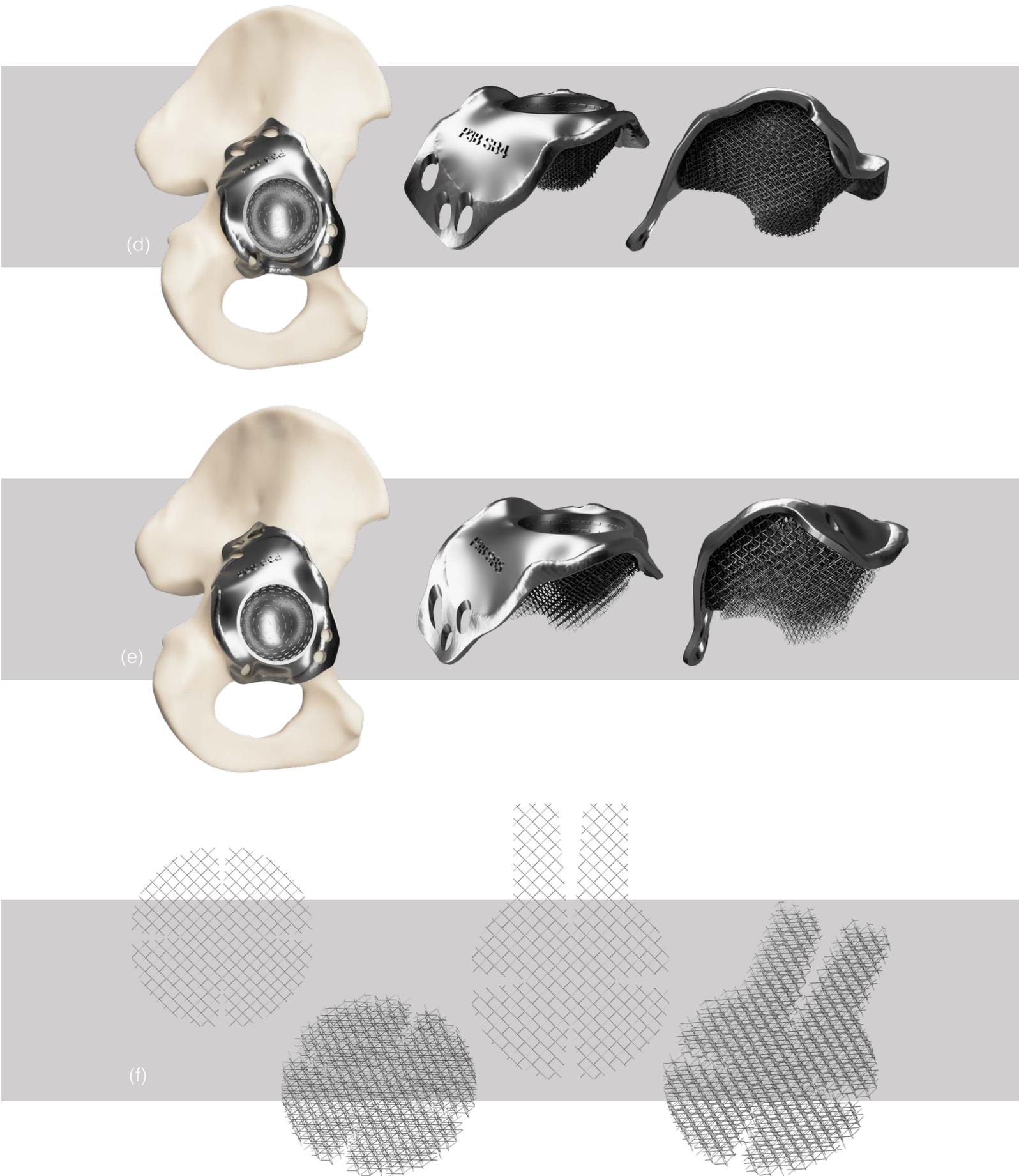
Figure 14: Rendered images of the designed acetabular cups; SB1 (a), SB2 (b), SB3 (c), SB4 (d), SB5 (e), deformable meshes (f).

Each cup was produced once by 3D Systems (Leuven, Belgium) using selective laser melting. For these cups the ProX DMP 320 (3D Systems, Leuven, Belgium) SLM machine was used.[31] The material is commercially pure titanium (Grade 1) in powder form.[29] The generic deformable meshes were produced two times each. The cups were tested as manufactured, the only post processing was support removal. The printed acetabular cups and meshes are shown in Figure 15, more pictures can be found in appendix Figure A 6.
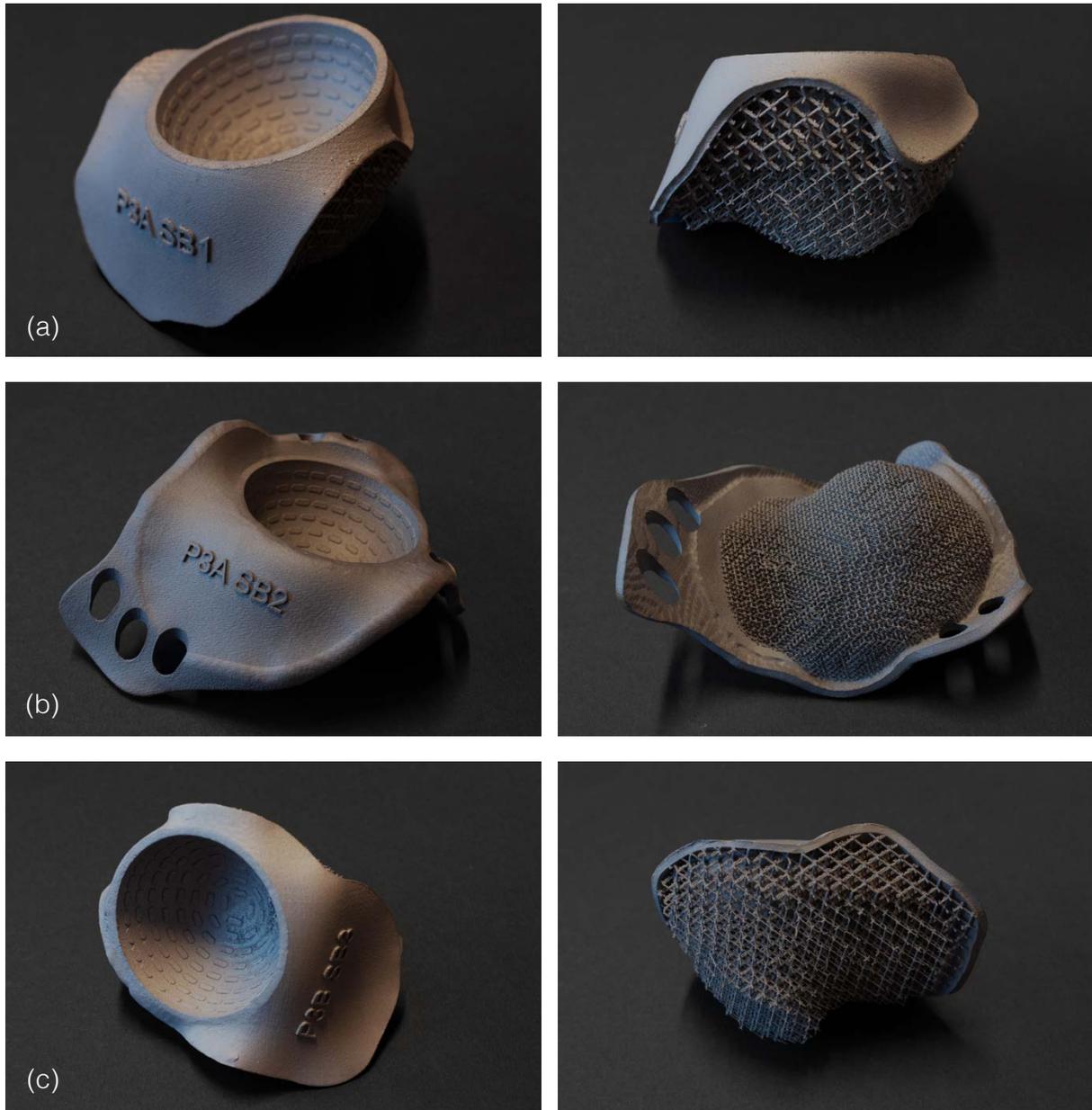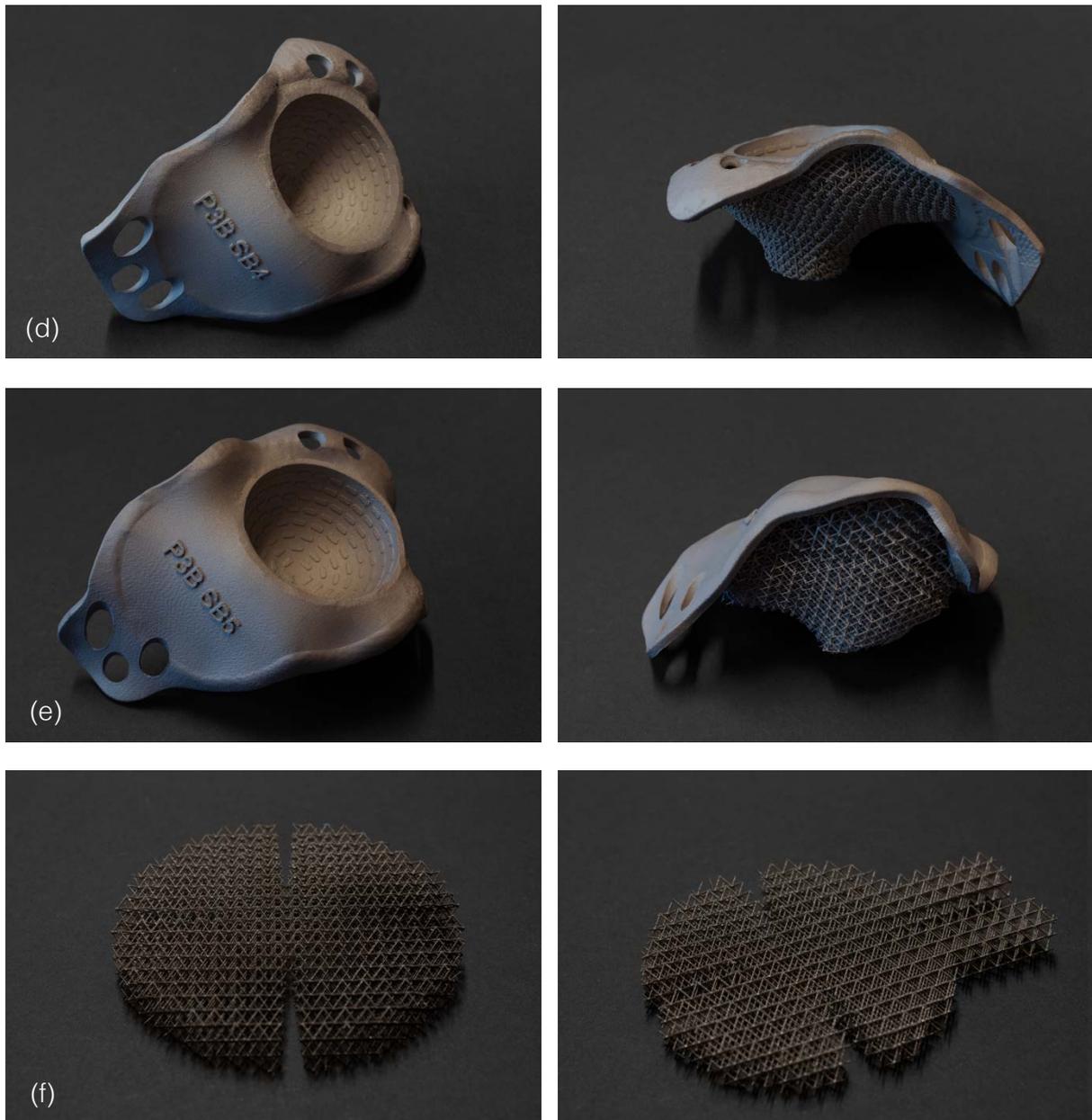
Figure 15: Photographs of the manufactured acetabular cups; SB1 (a), SB2 (b), SB3 (c), SB4 (d), SB5 (e), deformable meshes (f).

The acetabular cups were inserted into their corresponding Sawbones hemipelves by Dr. H.CH. Vogely and Dr. B.C.H. van der Wal, two orthopaedic surgeons at the UMC Utrecht. To insert the cups, a standard hip insertion set from the operating room was used. The oversized acetabular cups were placed into position and subsequently inserted using an inserter and hammer. The two undersized cups needed a mesh to fill the medial gap between the implant and Sawbones interface. All three sizes circular and generic meshes were available to the surgeons to be used in combination with the undersized acetabular cups. For these cups the generic mesh was placed into position first and partially deformed using a hammer and inserter. Then the acetabular cup was placed and inserted with the inserter and hammer, further deforming the generic mesh underneath.

After insertion of the acetabular cups the liners were cemented into the cups using Zimmer Biomet Refobacin R® bone cement.[49] The Sawbones hemipelves with inserted acetabular cups and cemented liners are shown in Figure 16.

Since the deformability of the oversized cups cannot be assessed during insertion, a CT scan was made after insertion (Philips IQon Spectral CT, metal artefact reduction protocol, UMC Utrecht). The slice thickness of the scan was 0.8 mm. To assess deformation of the oversized cups the DICOM files were segmented using the Mimics Medical software package (Version 24, Materialise, Belgium). The registered scans were positioned on the original CAD (Computer Aided Design) file using a point to point registration method, this was done using the 3-Matic software package (Version 13, Materialise, Belgium). All registered points were positioned at the solid (non-deformable) part of the acetabular cups.
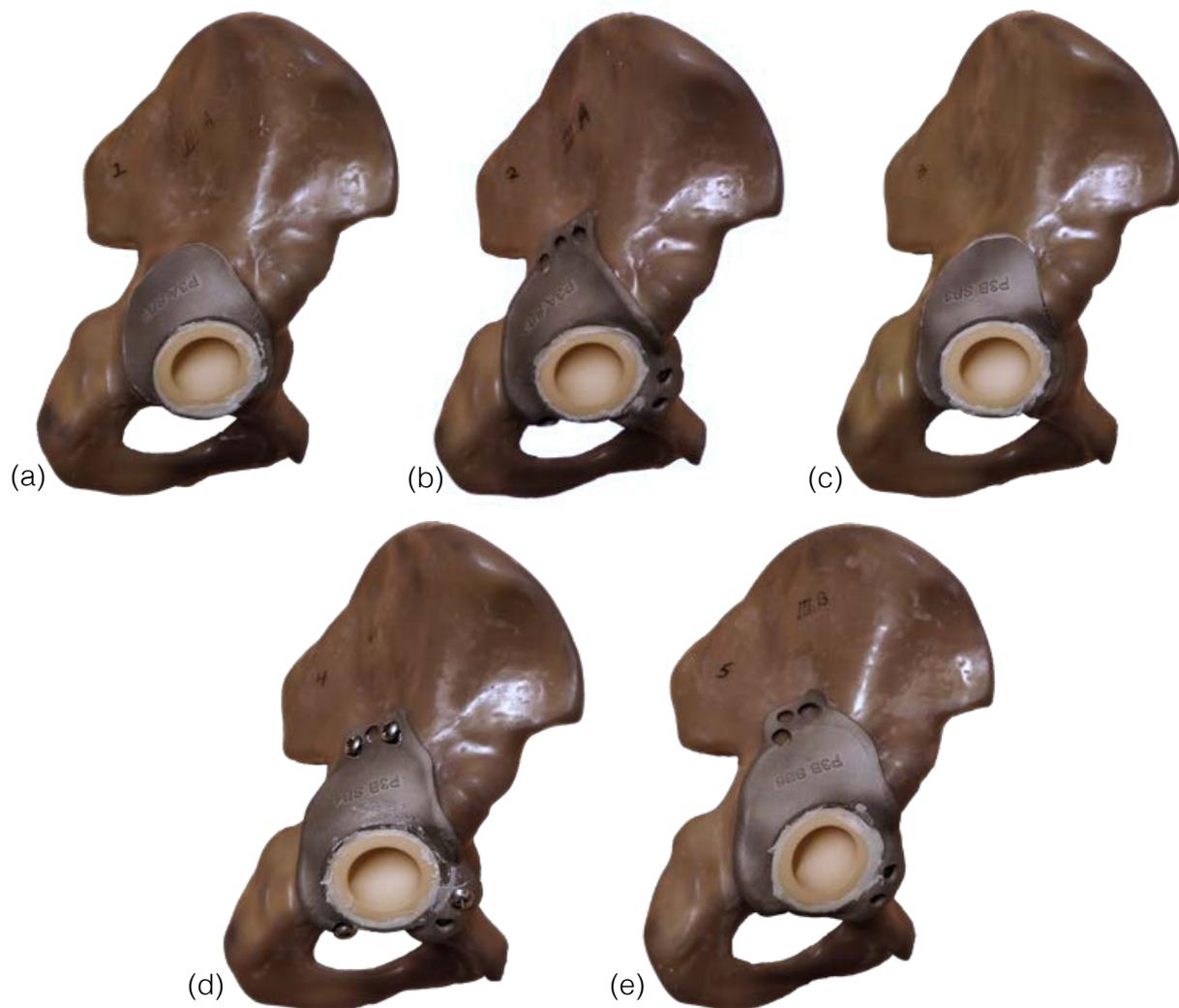
Figure 16: Photographs of the inserted acetabular cups. SB1 (a), SB2 (b), SB3 (c), SB4 (d) and SB5 (e).

3.2.4 Mould and femoral head

To position the hemipelves during mechanical testing a mould was designed to place them in 180° anterior pelvic plane. The force vector acting on the hemipelves, described by Bergmann *et al.* is in line with the direction of compression when placed in the mould.[50] The mould was designed using the 3-Matic software package (Version 13, Materialise, Leuven, Belgium). This mould was then hollowed in CAD with a wall thickness of 4 mm. This part was 3D printed (Oceanz, Ede, Netherlands) out of PA12 using selective laser sintering (SLS). To ensure rigidity of the mould the hollow cavity was filled with

epoxy resin. (Polyservice, Amsterdam, Netherlands) The mould is designed in a way that the Sawbones hemipelves can be inserted into the mould in the direction of compression testing. The mould and direction of insertion of the hemipelves is shown in Figure 17.

A 28 mm femoral head was fitted to a solid metal connection bar by the MTKF (UMC Utrecht, Netherlands) which can be clamped in the upper vice of the testing machine.

Figure 17: Rendered images of the mould for cyclic testing with the placement of the Sawbones hemipelves.

3.2.5 Mechanical testing

All Sawbones hemipelves with acetabular cups were cyclically tested on a Lloyd LS 5 universal testing machine (Amatek, Berwyn, United States). The mould was clamped onto the lower compression plate, then a hemipelvis with prior inserted acetabular cup was placed into the mould. The acetabular head was placed into the upper clamp and positioned into the liner. A preload of 100 N was used to keep pressure on the pelvis. A picture of the test setup can be seen in Figure 18.

All acetabular cups were first tested up to 1000 cycles with a force altering between 100 N and 1800 N to simulate a walking motion. A minimum load of 100 N was used to ensure the acetabular head did not lose contact with the liner. The maximum compressive force of 1800 N is based on the average peak load for walking.[50] The extension speed of the machine was kept constant at 60 mm/min. After 1000 cycles a second test of 50 cycles was performed.

The output of the cyclic compression test is a time-extension curve. The difference in machine extension between the first cycle and the last cycle gives the extra penetration of the femoral head.
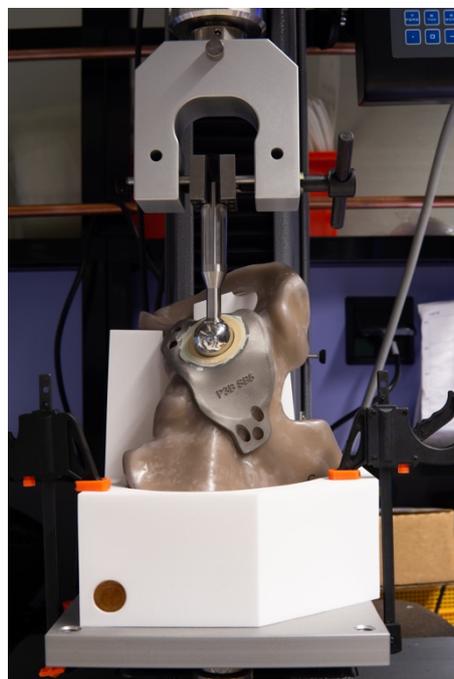
Figure 18: Test setup of the cyclic tests for the acetabular cups.

3.3 Results

3.3.1 Insertion of the acetabular components

All five acetabular cups were implanted into the matching Sawbones hemipelves. Subjectively, according to both surgeons none of the cups did require a noticeably larger impact force to insert them than a regular hemispherical acetabular cup. Only the smallest generic meshes (53 mm) were used with the undersized cups, one circular and one elongated mesh. The elongated mesh was cut to size with plain scissors to fit the defect.

In both cups without flanges the deformation was less than planned in the ischium direction, evident from a small gap between the solid part of the cup and the Sawbones cortex.

One generic mesh (Paprosky type 3B defect) broke when deformed with an inserter. Also broken titanium struts fell through the defect in the medial wall when the undersized flanged cup was inserted. Some broken and loose struts were observed in other cups judged by the sound of rattling metal in the porous section of the cup.

Only one acetabular cup needed additional fixation with screws after insertion, this was the cup with the broken generic mesh (Paprosky type 3B defect). None of the other cups could be removed by hand after insertion.

To assess the deformation of the oversized acetabular cups a CT scan was made (Philips IQon Spectral CT, metal artefact reduction protocol, UMC Utrecht). Registration of the CT scan onto the original CAD file shows the deformation of the outer porous layer of all three oversized acetabular cups, this can be seen in Figure 19.
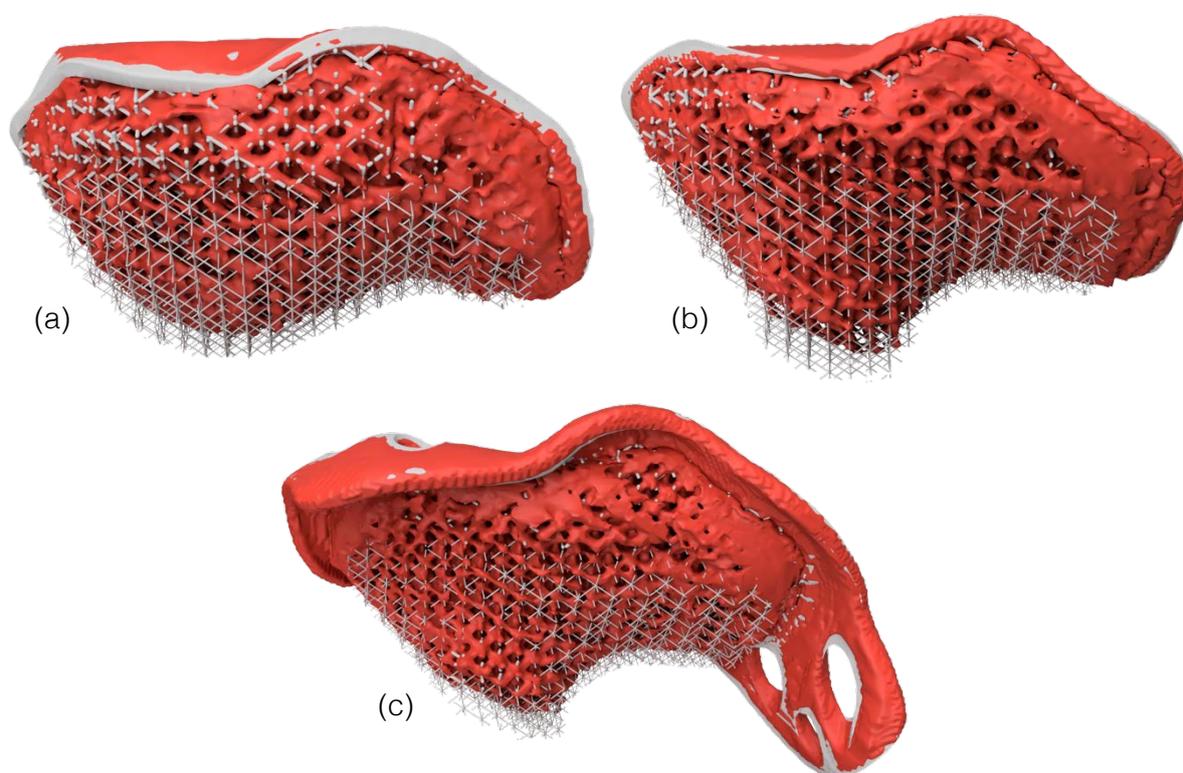
Figure 19: Rendered images of the CT-CAD registration; SB1 (a), SB3 (b), SB5 (c). The red part is the segmented cup after insertion, the grey part is the original CAD file.

3.3.2 Mechanical testing

All five acetabular cups, inserted in Sawbones hemipelves, were cyclically tested up to 1000 cycles. With this cyclic compression a walking motion was simulated. The time-extension plot for SB1 is shown in Figure 20. The time-extension curves for the other cups can be found in appendix Figure A 8-Figure A 11. The curves show that the machine extension increases during the first cycles to reach 1800 N, indicating a displacement. The more cycles performed the more the curve flattens. This is true for all acetabular cups. The second test of 50 cycles shows this behaviour to a lesser extent.

The machine extension needed to reach 1800 N at the first, second and last compression are visualised in Figure 20. The extension of the first compression is indicated by the lower red line, the second compression by the yellow line the last compression by the upper red line. The difference in extension between the first and last compression and the second and last compression is shown in Table 6. This is the additional penetration of the femoral head. The same is done for the second test of 50 cycles for the first and last compression, indicated by the red lines.
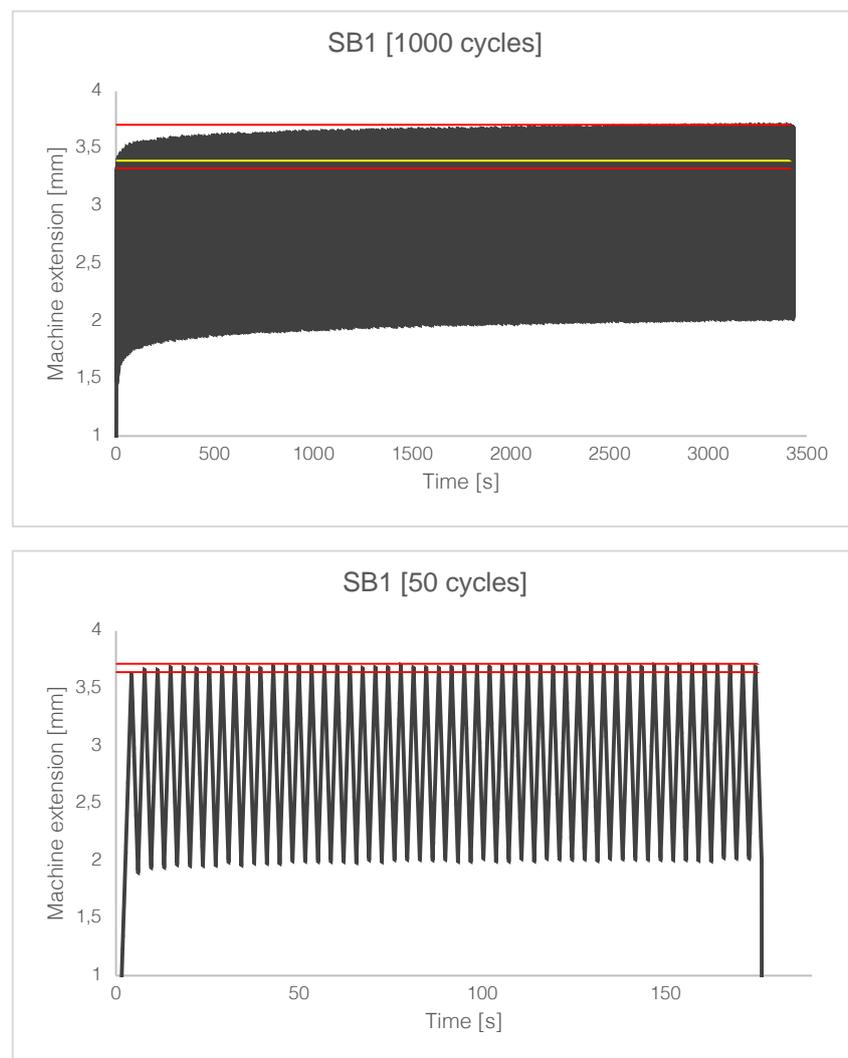
Figure 20: Time-extension curves for the 1000 and 50 cycles test for SB1. The extension of the first compression is indicated by the lower red line, the second compression by the yellow line the last compression by the upper red line. For the second test of 50 cycles only the first and last compression are shown.

When comparing the deformation between the first and last compression SB1 showed the most additional femoral head penetration (0.3793 mm) under cyclic compression. SB4 showed the lowest additional femoral head penetration (0.1781 mm). During the second test with 50 cycles all cups showed less femoral head penetration than during the first test. However, SB1 still showed the most penetration (0.0726 mm) and SB4 the least (0.0197 mm).

Table 6: Values of the femoral head penetration for both the 1000 and 50 cycles test. The differences are measured between the first and last compression and the second and last compression.

Acetabular cup	1000 cycles		50 cycles
	First-last compression [mm]	Second-last compression [mm]	First-last compression [mm]
SB1	0.3793	0.3120	0.0726
SB2	0.2190	0.1973	0.0264
SB3	0.2281	0.1867	0.0260
SB4	0.1781	0.1406	0.0197
SB5	0.2610	0.2193	0.0275

3.4 Discussion

Five 'patient specific' acetabular cups were designed and inserted in Sawbones hemipelves with Paprosky type 3A and 3B acetabular defects. A mould was designed to position the hemipelves in 180° anterior pelvic plane for cyclic testing. The acetabular cups were cyclically tested up to 1000 cycles (simulating a walking motion) to assess additional femoral head penetration under cyclic loading.

During the cyclic tests all implants showed additional penetration of the femoral head between the first and last compression up to 1800 N. This happened in both the first and second cyclic test. However, the penetration was about a factor 10 less during the second compression test of 50 cycles. We hypothesize the implants 'settle' during the first cycles in which some extra deformation takes place. In literature this is also described as 'bedding-in' of the implant.[51] The extra penetration of the femoral head between the first compression and last compression is between 0.1781 and 0.3793 mm in this test. Saffarini *et al.* describes values between 0.05 and 0.27 mm of femoral head penetration for cementless hemispherical cups.[52] Also the graphical illustration of femoral head penetration over time in this study is consistent with the curves from our experiments.

Insertion of the acetabular cups was performed without major complications. Subjectively, both surgeons did not use noticeably more force to insert the deformable cups than regular hemispherical cups. The solid part of the cups without flanges was designed to be flush with the cortical shells of the Sawbones hemipelves. However, in the direction of the ilium there still was a small gap between the solid part of the cup and the cortical shell. This indicates the acetabular cup did not deform as anticipated. This can be explained by the fact that the cup is inserted using a hemispherical inserter which is positioned in the cup, which is not the centre of the implant. The impact of the hammer is therefore not evenly distributed.

A way to resolve this is creating a second impact point, directed towards the ilium. Another solution could be to reduce the thickness of the deformable layer in the ilium direction. Also, the deformable mesh in SB3 penetrated the defect in the medial wall. This can be easily resolved in the design of the cup.

In SB4, an undersized flanged cup with separate deformable mesh, the mesh broke during insertion of the mesh. The decision was made to not replace the mesh but to use the already inserted, broken one. The SB4 cup was the only cup that needed additional fixation with screws. It cannot be said if the cup was not fixed properly because the mesh was broken or that a separate mesh doesn't work in combination with defects in the medial wall.

After insertion of the acetabular cups with attached deformable layer (SB1, SB3, SB5), there were two possibilities; either the deformable layer deformed and filled the acetabular defect or the struts penetrated the Sawbones solid foam which represents the trabecular bone. The CT scan that was made after insertion showed that the deformable layer indeed deformed. However, this is only a global deformation since the spatial resolution of the CT scan does not allow for segmentation of individual struts due to the partial volume effect.[53] A μCT scan, also used to show three-dimensional trabecular bone structures, has a spatial resolution ranging from 20 to 100 μm which would be suitable to show individual struts.[54,55] However, there is limited physical space in the μCT scanner and the Sawbones hemipelves with inserted acetabular cups were too large to scan at once.

After insertion of the acetabular cups broken struts could be shaken out of the Paprosky type 3B defect hemipelves through the defect in the medial wall. Broken struts could be heard rattling in the Paprosky type 3A defect hemipelves when shaken. There is no doubt that the implant should remain one construct

when clinically used. Also, these acetabular cups were tested as manufactured without additional post processing, except for support material removal. HIP treatment would increase ductility for CP-Ti.[29,38] Greater ductility should theoretically reduce the chance of strut breakage. Another method to prevent broken struts could be decreasing the thickness of the deformable layer.

All acetabular cups were cyclically tested after insertion with two cyclic tests. The first test consisted of 1000 cycles and the second test of 50 cycles. During the first test of SB3 the testing machine had an unintentional error at ±900 cycles and stopped. The remaining cycles were performed directly after resetting the machine before the second test was conducted. As far as we can tell this had no noticeable influences on the results.

The use of Sawbones hemipelves comes with its limitations. The inner solid foam that represents trabecular bone is isotropic, where trabecular bone in the human pelvis can be considered as largely transversely isotropic.[42] Also the yield strength of human pelvic trabecular bone is a factor 3 to 10 lower than the yield strength of the Sawbones solid foam (Table 4). However, next to cadaveric in-vivo testing this is the nearest resemblance of the physiological situation.

SB1 showed the most additional femoral head penetration of all acetabular cups, this is not in line with the expectations since this cup was inserted in an acetabular defect with an intact medial wall. An explanation for this could be that this was the first cup inserted, suggesting some sort of learning curve in insertion. SB4, the cup with the broken deformable mesh, was the acetabular cup that showed the least additional femoral head penetration. This cup was additionally fixated with screws and thus stiffened the whole pelvis with implant. This could have played a part in the fact that SB4 showed the least additional femoral head penetration during the cyclic test.

The data obtained in part one was a good basis for designing the acetabular cups. Both the elastic modulus and yield strength of the 4x4x4 mm unit cell size (0.2 mm strut thickness), which was used for the deformable section, are lower than the respective moduli of human pelvic trabecular bone. Since the oversized cups did deform upon insertion and are almost positioned as planned, we can assume there is 4 mm deformation in the deformable layer. This is about 50% strain in the deformable layer. According to the data in Figure 6 this means all deformation of the plateau region took place and material densification is taking place. This extend of material densification could be the cause of the broken struts, μCT images will be relevant to accurately visualize the deformation.

3.5 Conclusion

The aim of this study was design and evaluate a new concept of acetabular cup with a highly porous plastically deformable component to fill large bone defects. This acetabular cup has the potential of diminishing stress shielding and stimulating the formation of bone.[18–22] The acetabular cups designed and tested in this study showed promising results. The deformable layer of the acetabular cups deformed during insertion, filling the acetabular cavity. Though insertion resulted in some broken struts. The cyclic test resulted in some additional penetration of the femoral head; the values found in the experiments are mostly in line with literature.[52] The concept of a deformable acetabular cup seems a feasible solution for treating large acetabular defects. The results of these experiments are a validation for further development of these implants.

4

Future work

Future work is needed to further develop the deformable acetabular cup concept. Though the Sawbones hemipelves were the best option available for these experiments, cadaveric experiments are recommended for further tests. The trabecular bone in the human pelvis has a lower yield strength than the solid foam used in the Sawbones hemipelves. Since the implants are very likely to be used in osteoporotic patients, cadaveric experiments are needed to validate the deformability of the porous layer in human pelvic bone.

All current acetabular cups are tested as manufactured. For further development of these implants it is recommended perform post processing to further optimize ductility.[29,38]

In this study a cyclic test was performed up to 1000 cycles due to machine and time constraints. Further cyclic testing is needed to assess the fatigue behaviour of these highly porous lattice structures. Some research on fatigue behaviour of CP-Ti lattice structures is already described in literature. Li *et al.* studied fatigue behaviour of titanium lattice structures with a porosity up to 70%.[56] Yavari *et al.* studied fatigue behaviour of higher porosity samples, up to 84%, but used samples manufactured of Ti6Al4V.[57] The samples used in this study have a porosity up to 97.5%, considerably higher than what is used in literature. It is important to remind that bone will grow into the porous part of the implant and will form a solid construct. This means that most of the cyclic loading is performed on the bone-lattice structure composite rather than the lattice structure alone.

This brings up one of the most important factors in implant longevity; biological fixation. It is important to evaluate the biological effects of these highly porous lattices on living bone. The outer layer of these highly porous lattices often-end in open ended struts due to the direct patterning approach used to create the lattices.[28] These open-ended struts are sharp. The interaction between these open-ended struts and the living bone tissue is something that requires further research.

5
References

1.   Kurtz S, Ong K, Lau E, Mowat F, Halpern M. Projections of Primary and Revision Hip and Knee Arthroplasty in the United States from 2005 to 2030. 2007:780-785. doi:10.2106/JBJS.F.00222

2.   Schmalzried TP, Kwong LM, Jasty M, et al. The mechanism of loosening of cemented acetabular components in total hip arthroplasty. Analysis of specimens retrieved at autopsy. *Clin Orthop Relat Res*. 1992;(274):60—78. http://europepmc.org/abstract/MED/1729024.

3.   Paprosky WG, Weeden SH, Bowling JW. Component removal in revision total hip arthroplasty. *Clin Orthop Relat Res*. 2001;(393):181-193. doi:10.1097/00003086-200112000-00021

4.   CHARLES ANDERSON Engh, WILLIAM L Griffin and CLM. Cementless Acetabular Components. *J Bone Joint Surg Br*. 1990;72(1):53-59. doi:10.2190/y2bt-xqh1-p0xc-1n91

5.   Won CH, Hearn TC, Tile M. Micromotion of cementless hemispherical acetabular components. *J Bone Jt Surg - Ser B*. 1995;77(3):484-489. doi:10.1302/0301-620X.77B3.7744942

6.   Bürkner A, Fottner A, Lichtinger T, et al. Primary stability of cementless threaded acetabular cups at first implantation and in the case of revision regarding micromotions as indicators. *Biomed Tech*. 2012;57(3):169-174. doi:10.1515/bmt-2011-0066

7.   Morsi E, Orth MS. Total Hip Arthroplasty With Shelf Grafts Using Uncemented Cups A Long-term Follow-up Study. 1996;11(1):81-85.

8.   Hooten JP, Engh CA, Heekin RD, Vinh TN. Structural bulk allografts in acetabular reconstruction: Analysis of two grafts retrieved at post-mortem. *J Bone Jt Surg - Ser B*. 1996;78(2):270-275. doi:10.1302/0301-620X.78B2.0780270

9.   Pulido L, Rachala SR, Cabanela ME. Cementless acetabular revision: Past, present, and future - Revision total hip arthroplasty: The acetabular side using cementless implants. *Int Orthop*. 2011;35(2):289-298. doi:10.1007/s00264-010-1198-y

10.   Paprosky WG, Perona PG, Lawrence JM. Acetabular defect classification and surgical reconstruction in revision arthroplasty. A 6-year follow-up evaluation. *J Arthroplasty*. 1994;9(1):33-44. doi:10.1016/0883-5403(94)90135-X

11.   Brown NM, Morrison J, Sporer SM, Paprosky WG. The Use of Structural Distal Femoral Allograft for Acetabular Reconstruction of Paprosky Type IIIA Defects at a Mean 21 Years of Follow-Up. *J Arthroplasty*. 2016;31(3):680-683. doi:10.1016/j.arth.2015.10.020

12.   Carroll FA, Kerry RM, Stockley I, Hoad-Reddick DA, Kerry RM, Stockley I. The survival of support rings in complex acetabular revision surgery. *J Bone Jt Surg - Ser B*. 2008;90(5):574-578. doi:10.1302/0301-620X.90B5.19789

13.   Babis GC, Sakellariou VI, Chatziantoniou AN, Soucacos PN, Megas P. High complication rate in reconstruction of Paprosky type IIIa acetabular defects using an oblong implant with modular side plates and a hook. *J Bone Jt Surg - Ser B*. 2011;93 B(12):1592-1596. doi:10.1302/0301-620X.93B12.27299

14.   Gaiani L, Bertelli R, Palmonari M, Vicenzi G. Total hip arthroplasty revision in elderly people with cement and Burch-Schneider anti-protrusio cage. *Chir Organi Mov*. 2009;93(1):15-19. https://www.scopus.com/inward/record.uri?eid=2-s2.0-79959355904&partnerID=40&md5=2e4ede5d4ba583237f133c3cb871203c.

15.   Borland WS, Bhattacharya R, Holland JP, Brewster NT. Use of porous trabecular metal augments with impaction bone grafting in management of acetabular bone loss. *Acta Orthop*. 2012;83(4):347-352. doi:10.3109/17453674.2012.718518

16.   Baauw M, Van Hellemondt GG, Spruit M. A custom-made acetabular implant for paprosky type 3 defects. *Orthopedics*. 2017;40(1):e195-e198. doi:10.3928/01477447-20160902-01

17.   Baauw M, Van Hooff ML, Spruit M. Current construct options for revision of large acetabular defects: A systematic review. *JBJS Rev*. 2016;4(11):e2. doi:10.2106/JBJS.RVW.15.00119

18.   Sumner DR. Long-term implant fixation and stress-shielding in total hip replacement. *J Biomech*.

2015;48(5):797-800. doi:10.1016/j.jbiomech.2014.12.021

19. Huiskes R, Weinans H, Van Rietbergen B. The relationship between stress shielding and bone resorption around total hip stems and the effects of flexible materials. *Clin Orthop Relat Res.* 1992;(274):124-134. doi:10.1097/00003086-199201000-00014

20. Huiskes R, Rulmerman R, Van Lenthe GH, Janssen JD. Effects of mechanical forces on maintenance and adaptation of form in trabecular bone. *Nature.* 2000;405(6787):704-706. doi:10.1038/35015116

21. Currey JD. *The Mechanical Adaptations of Bones.* Princeton university press; 1984.

22. Turner CH, Pavalko FM. Mechanotransduction and functional response of the skeleton to physical stress: The mechanisms and mechanics of bone adaptation. *J Orthop Sci.* 1998;3(6):346-355. doi:10.1007/s007760050064

23. Zadpoor AA, Malda J. Additive Manufacturing of Biomaterials, Tissues, and Organs. *Ann Biomed Eng.* 2017;45(1):1-11. doi:10.1007/s10439-016-1719-y

24. Groenewoud A. Mechanical properties and deformation behaviour of highly porous pure titanium structures. 2018;(January).

25. de Jonge C. Deformable Acetabular Implants. 2019.

26. Wauthle R, Ahmadi SM, Amin Yavari S, et al. Revival of pure titanium for dynamically loaded porous implants using additive manufacturing. *Mater Sci Eng C.* 2015;54:94-100. doi:10.1016/j.msec.2015.05.001

27. Mazur M, Leary M, Sun S, Vcelka M, Shidid D, Brandt M. Deformation and failure behaviour of Ti-6Al-4V lattice structures manufactured by selective laser melting (SLM). *Int J Adv Manuf Technol.* 2016;84(5-8):1391-1411. doi:10.1007/s00170-015-7655-4

28. Tao W, Leu MC. Design of lattice structure for additive manufacturing. *Int Symp Flex Autom ISFA 2016.* 2016;(August 2016):325-332. doi:10.1109/ISFA.2016.7790182

29. Gr LT. LaserForm Ti Gr1 (A) LaserForm ® Ti Gr1 (A). 1:5-6.

30. 3D SYSTEMS. LaserForm ® Ti Gr5 (A). 2019;5(grade 23):5-6. https://fr.3dsystems.com/materials/metal.

31. 3D SYSTEMS. Metal Additive Manufacturing with the ProX ® DMP 3D printers METAL ALLOYS FOR THE PROX ® DMP 100 , 200 , 300. 2018:3-6.

32. Rombouts, M.; Kruth, J.P.; Froyen, L. and Mercelis P. Fundamentals of Selective Laser Melting of alloyed steel powders. *CIRP Ann.* 2006;55(1):187-192.

33. Kruth JP, Mercelis P, Van Vaerenbergh J, Froyen L, Rombouts M. Binding mechanisms in selective laser sintering and selective laser melting. *Rapid Prototyp J.* 2005;11(1):26-36. doi:10.1108/13552540510573365

34. Zadpoor AA. Mechanical performance of additively manufactured meta-biomaterials. *Acta Biomater.* 2019;85:41-59. doi:10.1016/j.actbio.2018.12.038

35. Campoli G, Borleffs MS, Amin Yavari S, Wauthle R, Weinans H, Zadpoor AA. Mechanical properties of open-cell metallic biomaterials manufactured using additive manufacturing. *Mater Des.* 2013;49:957-965. doi:10.1016/j.matdes.2013.01.071

36. Genovese K, Leeflang S, Zadpoor AA. Microscopic full-field three-dimensional strain measurement during the mechanical testing of additively manufactured porous biomaterials. *J Mech Behav Biomed Mater.* 2017;69(August 2016):327-341. doi:10.1016/j.jmbbm.2017.01.010

37. Ho KH, Newman ST, Rahimifard S, Allen RD. State of the art in wire electrical discharge machining (WEDM). *Int J Mach Tools Manuf.* 2004;44(12-13):1247-1259. doi:10.1016/j.ijmachtools.2004.04.017

38. Atkinson H V., Davies S. Fundamental aspects of hot isostatic pressing: An overview. *Metall Mater Trans A Phys Metall Mater Sci.* 2000;31(12):2981-3000. doi:10.1007/s11661-000-0078-2

39. Chong ACM, Miller F, Buxton M, Friis EA. Fracture toughness and fatigue crack propagation rate of short fiber reinforced epoxy composites for analogue cortical bone. *J Biomech Eng.* 2007;129(4):487-493. doi:10.1115/1.2746369

40. Szivek JA, Thomas M, Benjamin JB. Characterization of a synthetic foam as a model for human cancellous bone. *J Appl Biomater.* 1993;4(3):269-272. doi:10.1002/jab.770040309

41. Sawbones. TEST MATERIALS AND COMPOSITE BONES composite bones for test and. www.sawbones.com.

42. Dalstra M, Huiskes R, Odgaard A, van Erning L. Mechanical and textural properties of pelvic trabecular bone. *J Biomech.* 1993;26(4-5):523-535. doi:10.1016/0021-9290(93)90014-6

43.   van Ladesteijn R, Leslie H, Manning WA, et al. Mechanical properties of cancellous bone from the acetabulum in relation to acetabular shell fixation and compared with the corresponding femoral head. *Med Eng Phys*. 2018;53:75-81. doi:10.1016/j.medengphy.2018.01.005

44.   Rho JY, Ashman RB, Turner CH. Young's modulus of trabecular and cortical bone material: Ultrasonic and microtensile measurements. *J Biomech*. 1993;26(2):111-119. doi:10.1016/0021-9290(93)90042-D

45.   Cezayirlioglu H, Bahniuk E, Davy DT, Heiple KG. Anisotropic yield behavior of bone under combined axial force and torque. *J Biomech*. 1985;18(1):61-69. doi:10.1016/0021-9290(85)90045-4

46.   Zimmer. Zimmer® Trabecular Metal™ Acetabular Revision System. 2010.

47.   Materialise. *Mimics Innovation Course*.; 2018.

48.   Materialise. Materialise aMace. https://www.materialise.com/en/medical/acetabular-hip-implant-amace. Published 2019.

49.   Zimmer Biomet. Biomet Bone Cement R. *Zimmer Biomet*. 2017:1-4. https://www.zimmerbiomet.com/content/dam/zimmer-biomet/medical-professionals/cement/biomet-bone-cement-r.

50.   Bergmann G, Graichen F, Rohlmann A, et al. Realistic loads for testing hip implants. *Biomed Mater Eng*. 2010;20(2):65-75. doi:10.3233/BME-2010-0616

51.   Christi, J., Sychterz, M.S.E., Anderson, C., Anthony Yang, B.S. and Charles A. Analysis of Temporal Wear Patterns of Porous-Coated Acetabular Components : Distinguishing Between True Wear and So-Called Bedding-in. *J Bone Jt Surg - Am Vol*. 1999;81(6).

52.   Saffarini M, Gregory T, Vandenbussche E. Quantification of clearance and creep in acetabular wear measurements. *Ann Transl Med*. 2016;4(7):1-8. doi:10.21037/atm.2016.03.39

53.   Peyrin F, Salome M, Cloetens P, Laval-Jeantet AM, Ritman E, Ruegsegger P. Micro-CT examinations of trabecular bone samples at different resolutions: 14, 7 and 2 micron level. *Technol Heal Care*. 1998;6(5-6):391-401. doi:10.3233/thc-1998-65-611

54.   Feldkamp LA, Goldstein SA, Parfitt MA, Jesion G, Kleerekoper M. The direct examination of three‐dimensional bone architecture in vitro by computed tomography. *J Bone Miner Res*. 1989;4(1):3-11. doi:10.1002/jbmr.5650040103

55.   Peyrin F, Houssard JP, Maurincomme E, et al. 3D display of high resolution vertebral structure images. *Clin Rheumatol*. 1994;13(SUPPL. 1):18-21.

56.   Li F, Li J, Huang T, Kou H, Zhou L. Compression fatigue behavior and failure mechanism of porous titanium for biomedical applications. *J Mech Behav Biomed Mater*. 2017;65(September 2016):814-823. doi:10.1016/j.jmbbm.2016.09.035

57.   Amin Yavari S, Wauthle R, Van Der Stok J, et al. Fatigue behavior of porous biomaterials manufactured using selective laser melting. *Mater Sci Eng C*. 2013;33(8):4849-4858. doi:10.1016/j.msec.2013.08.006

6
Appendix
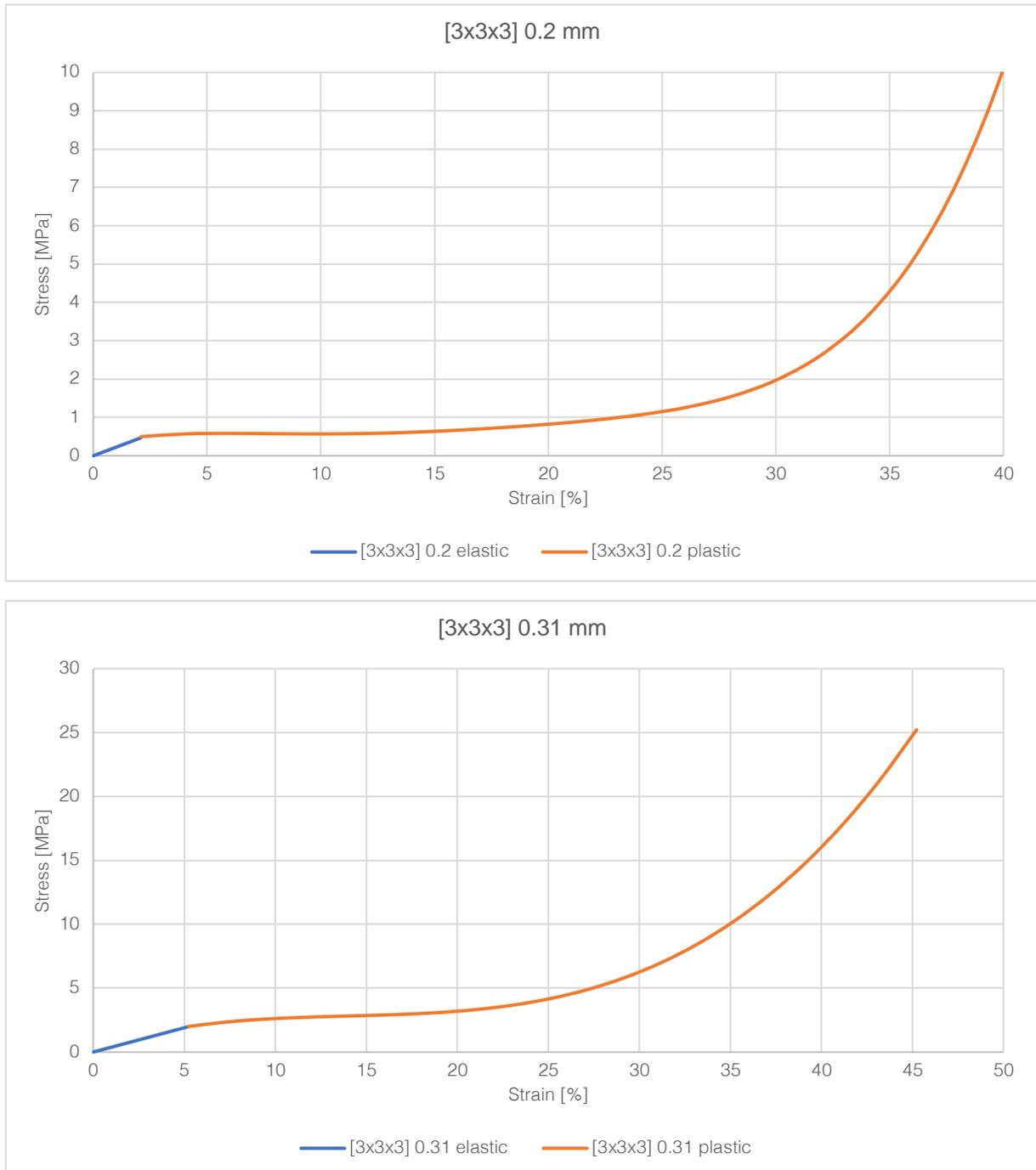
Figure A 1: The elastic and plastic data extracted from the cylindrical sample compression test of the 3x3x3 mm sample with a 0.2 mm (top) and 0.31 mm (bottom) strut thickness.
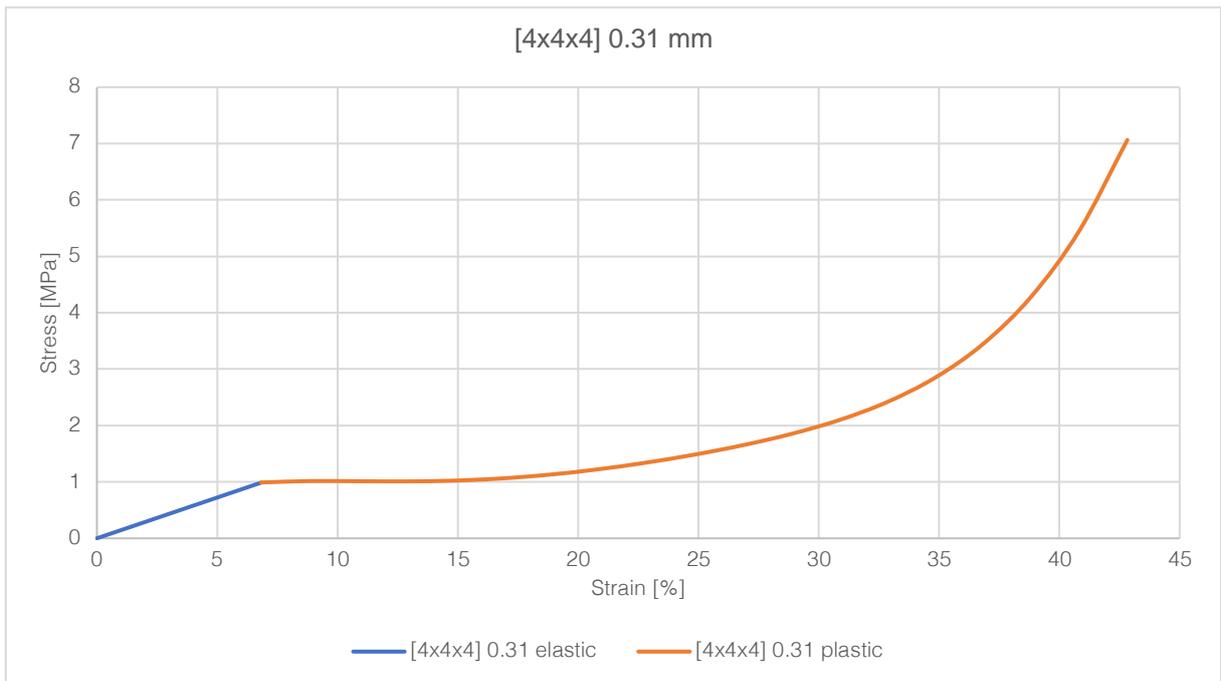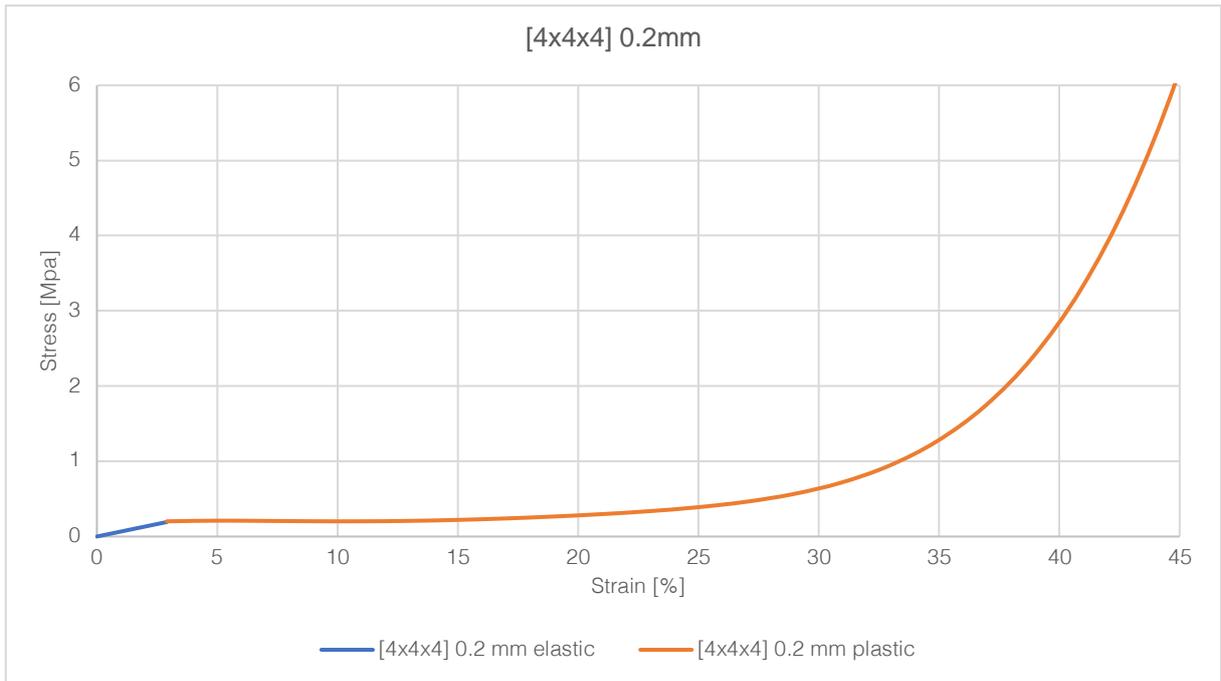
Figure A 2: Figure A 3: The elastic and plastic data extracted from the cylindrical sample compression test of the 4x4x4 mm sample with a 0.2 mm (top) and 0.31 mm (bottom) strut thickness.

[5x5x5] 0.2 mm

Stress [MPa] vs Strain [%]

[5x5x5] 0.2 elastic   [5x5x5] 0.31 plastic

[5x5x5] 0.31 mm

Stress [MPa] vs Strain [%]

[5x5x5] 0.31 elastic   [5x5x5] 0.31 plastic
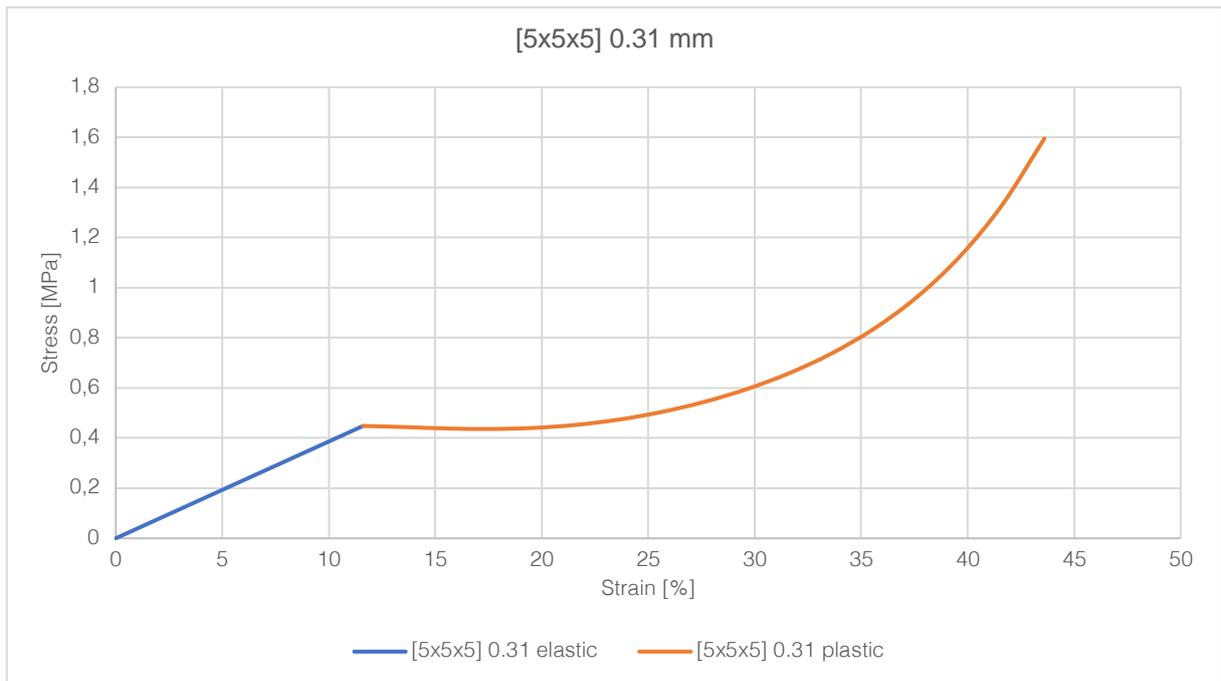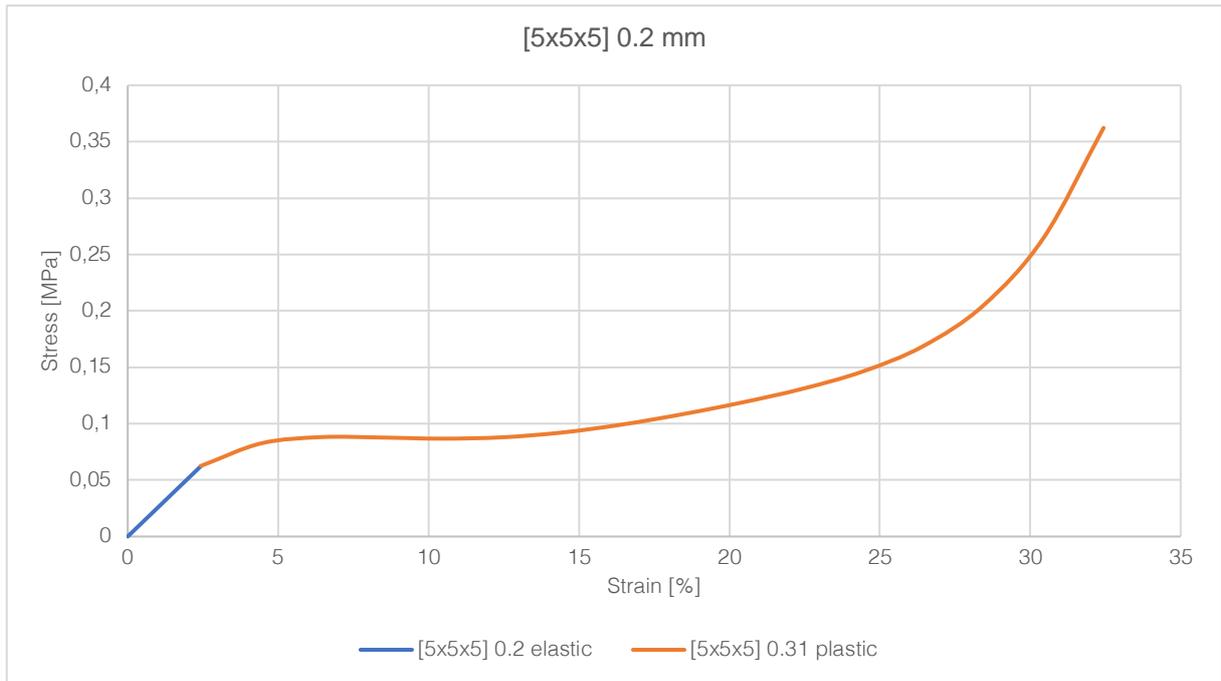
Figure A 4: Figure A 5: The elastic and plastic data extracted from the cylindrical sample compression test of the 5x5x5 mm sample with a 0.2 mm (top) and 0.31 mm (bottom) strut thickness.

(a)

(b)

(c)

(d)

(e)
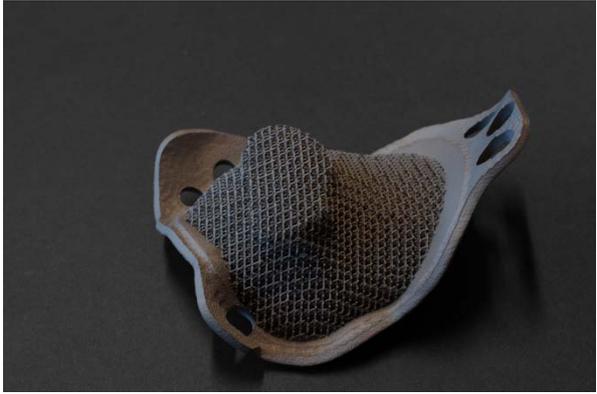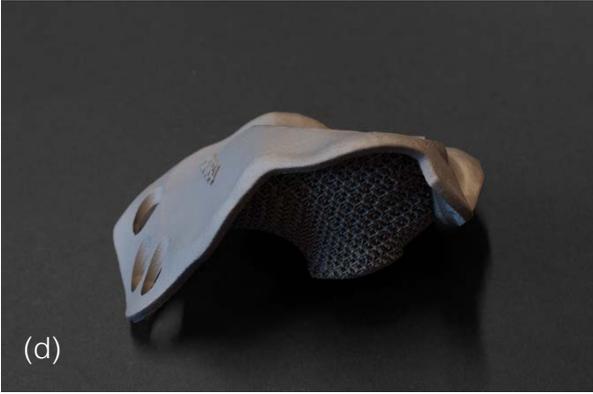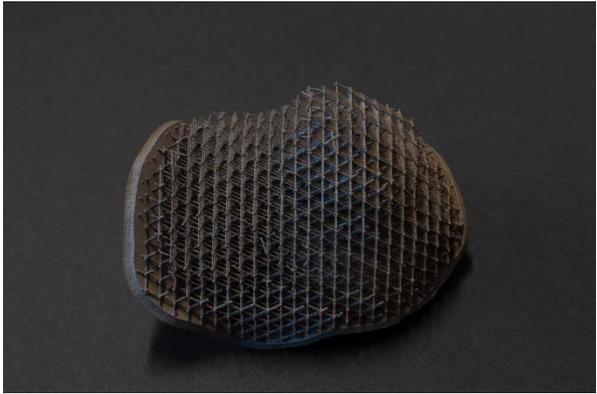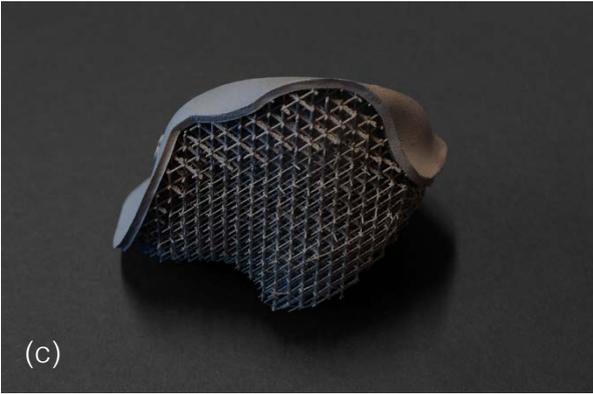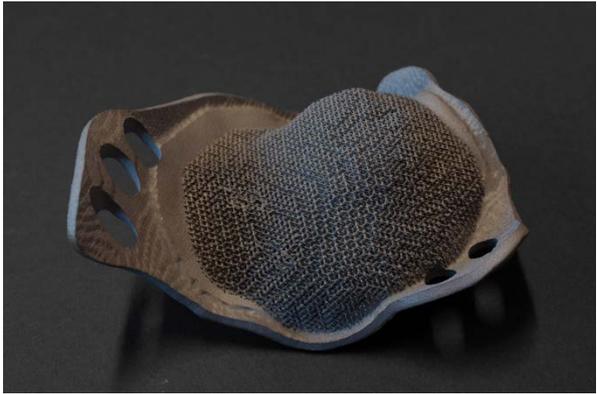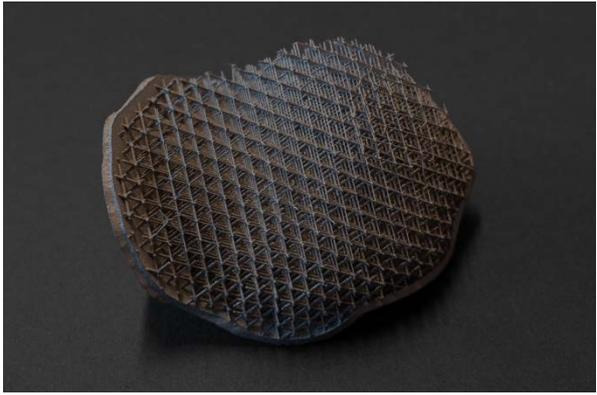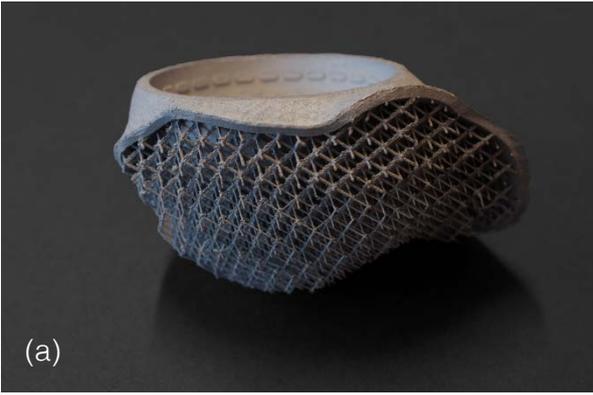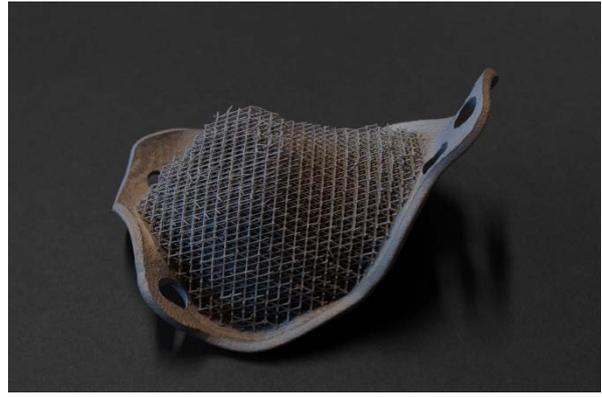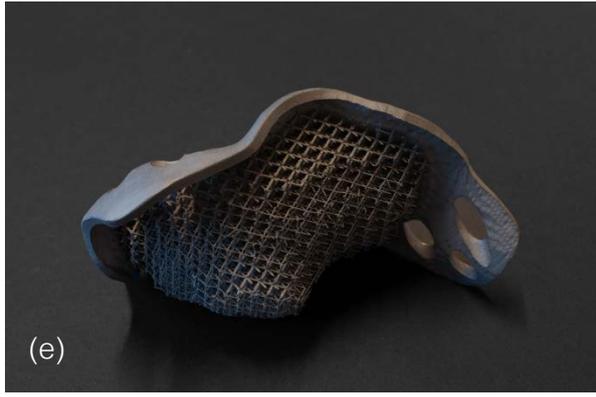
Figure A 6: Photographs of the manufactured acetabular cups; SB1 (a), SB2 (b), SB3 (c), SB4 (d), SB5 (e).
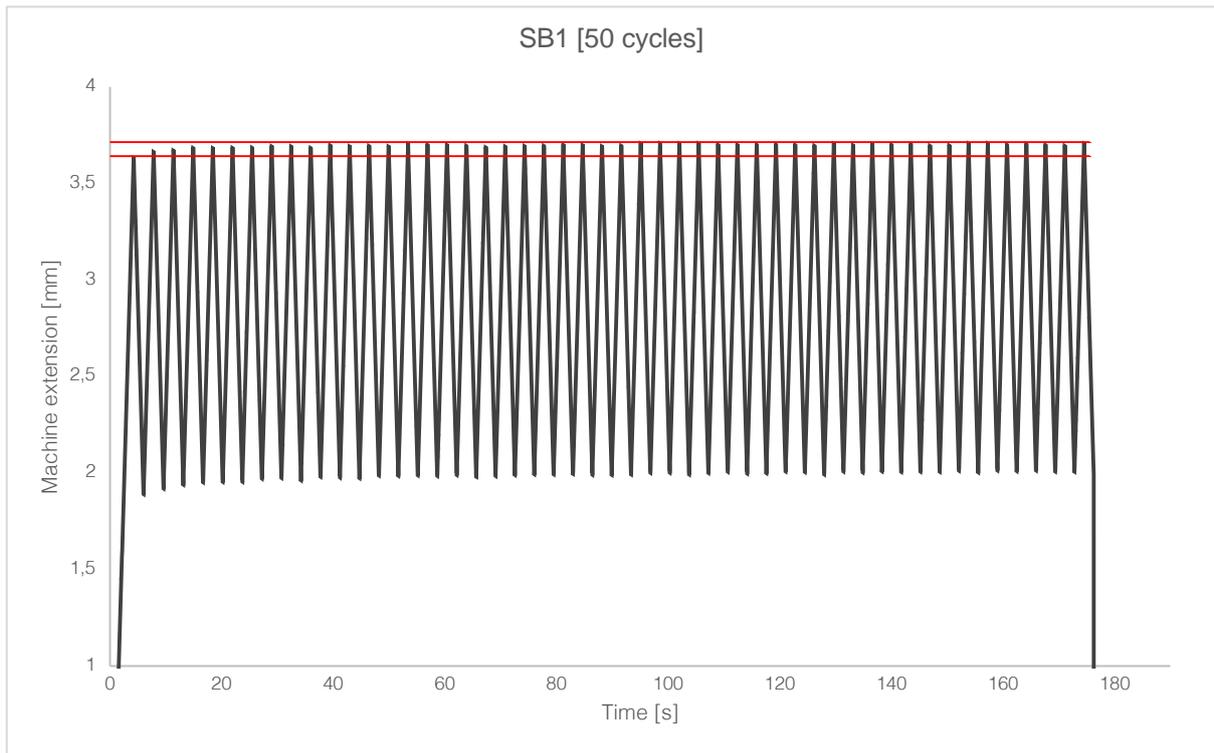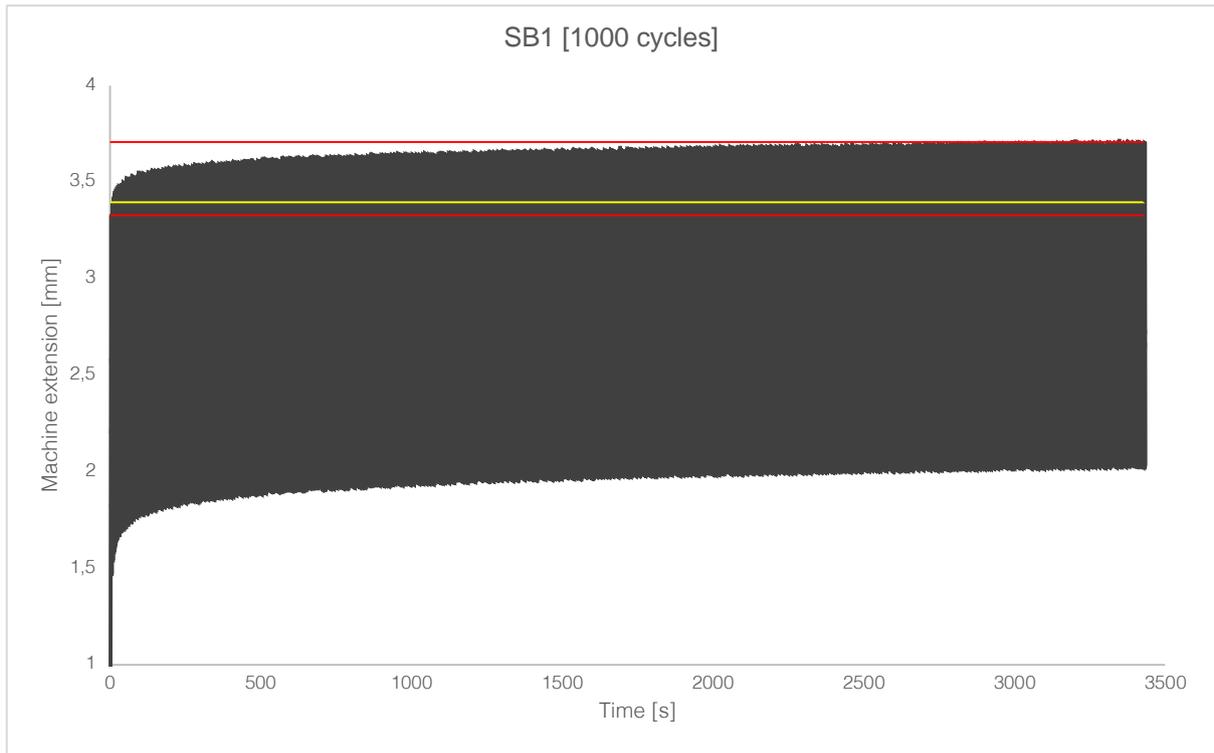
Figure A 7: Time-extension curves for the 1000 and 50 cycles test for SB1. The extension of the first compression is indicated by the lower red line, the second compression by the yellow line the last compression by the upper red line. For the second test of 50 cycles only the first and last compression are shown.
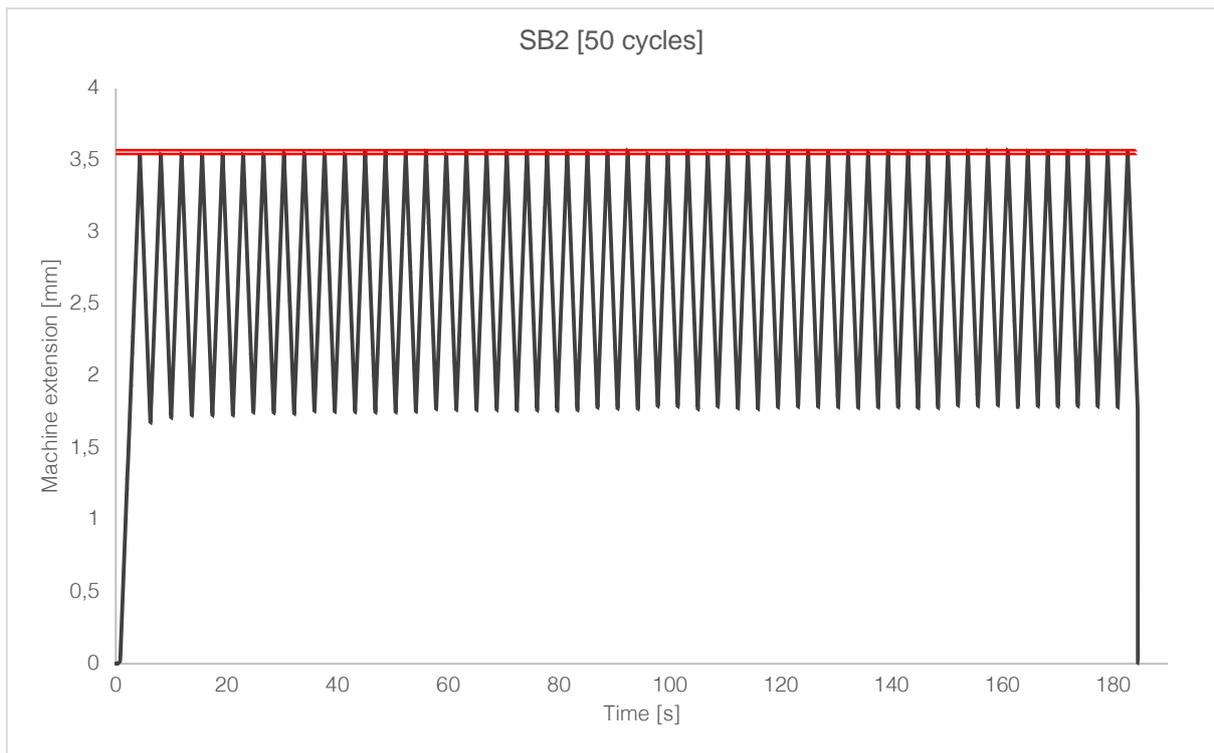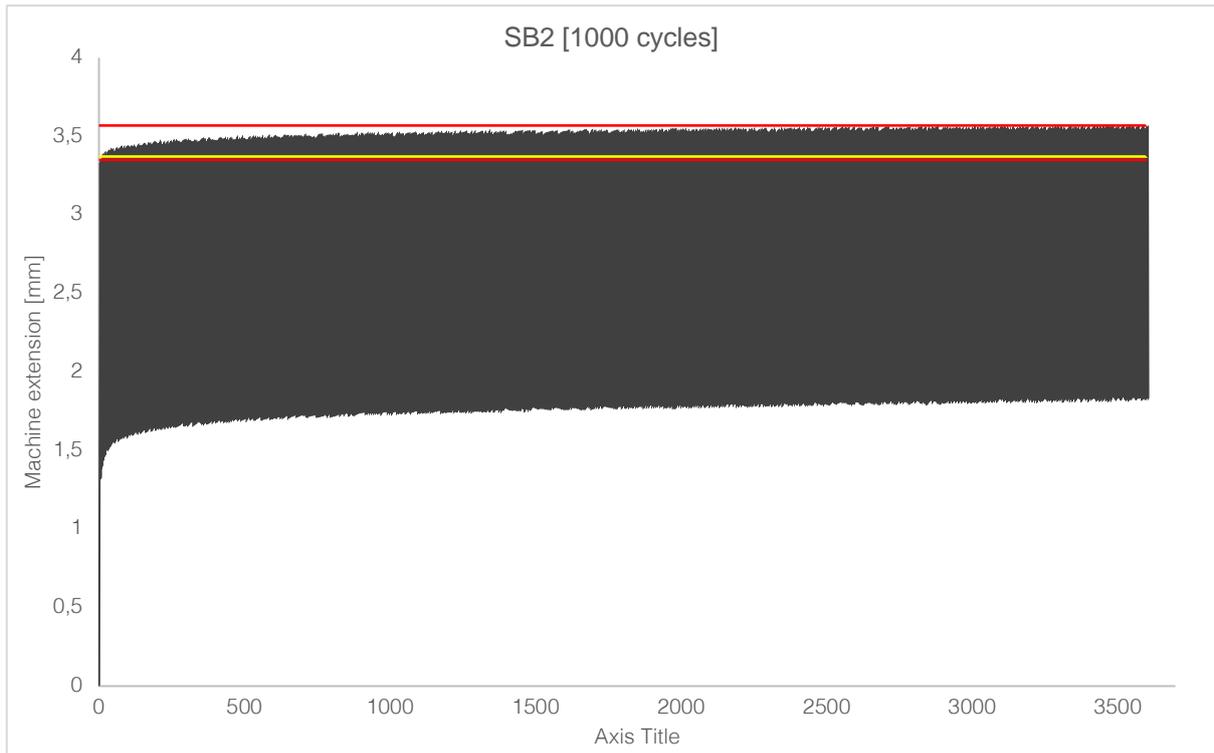
Figure A 8: Time-extension curves for the 1000 and 50 cycles test for SB2. The extension of the first compression is indicated by the lower red line, the second compression by the yellow line the last compression by the upper red line. For the second test of 50 cycles only the first and last compression are shown.
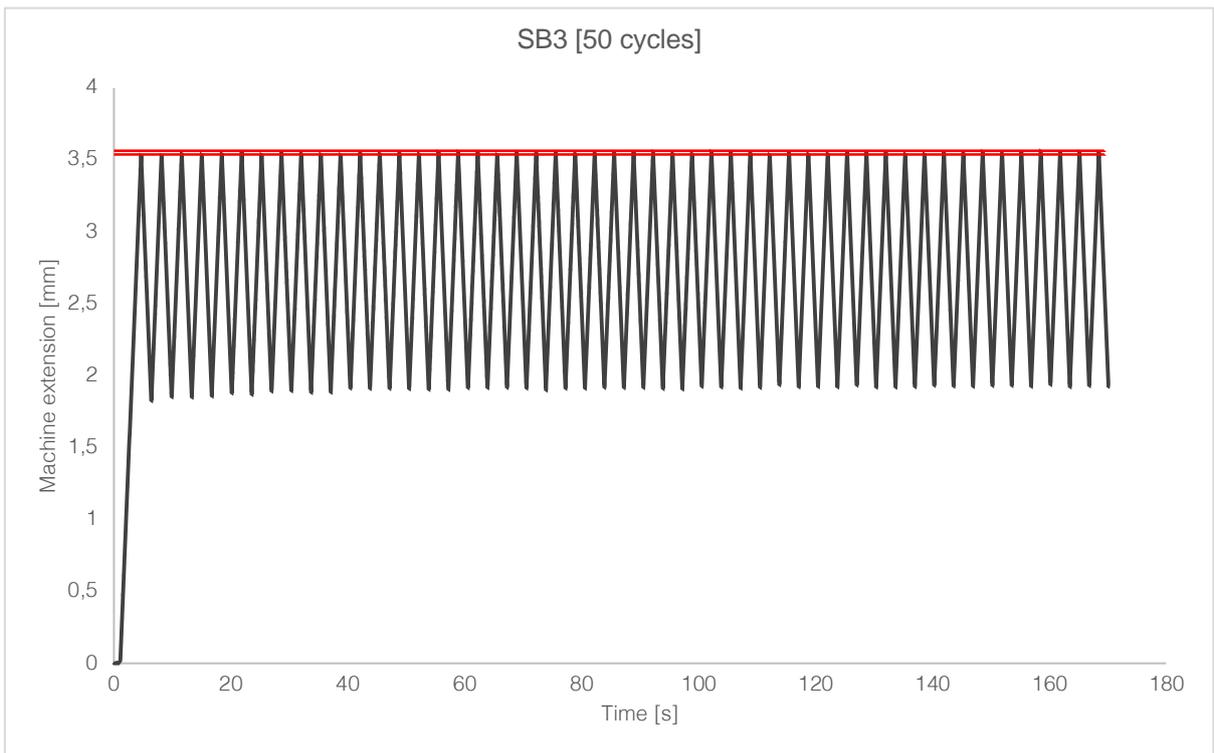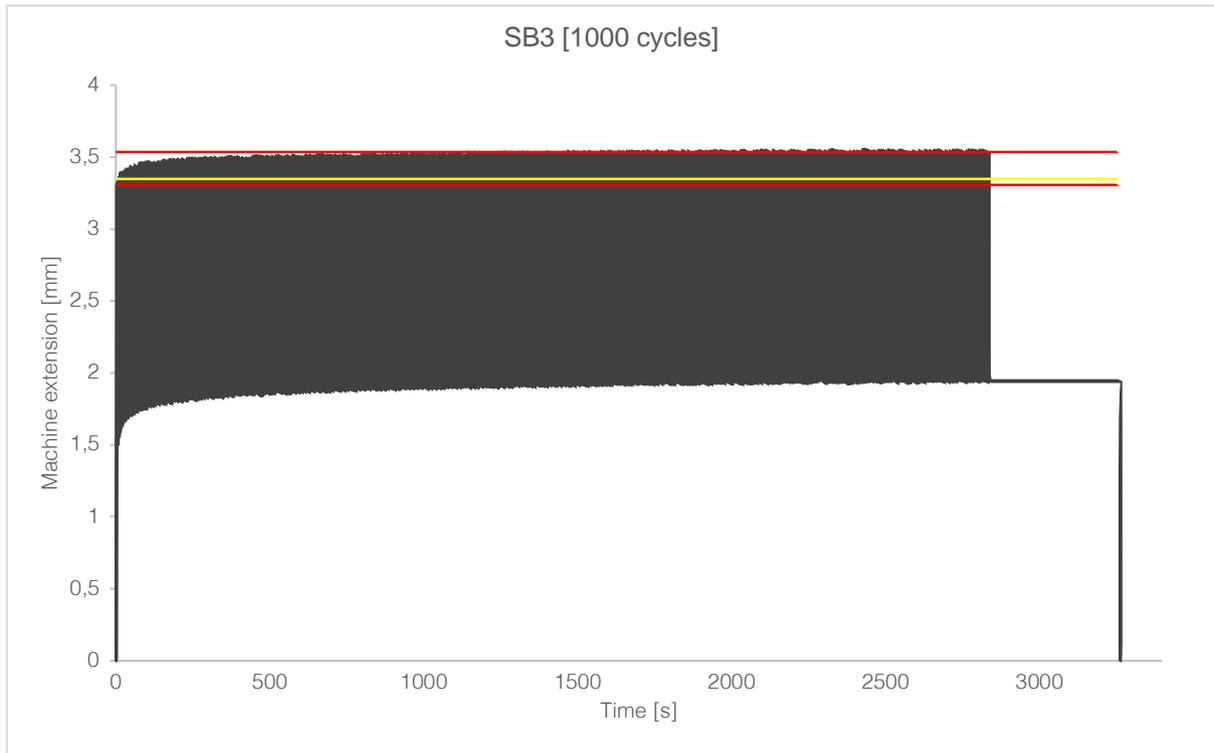
Figure A 9: Time-extension curves for the 1000 and 50 cycles test for SB3. The extension of the first compression is indicated by the lower red line, the second compression by the yellow line the last compression by the upper red line. For the second test of 50 cycles only the first and last compression are shown.
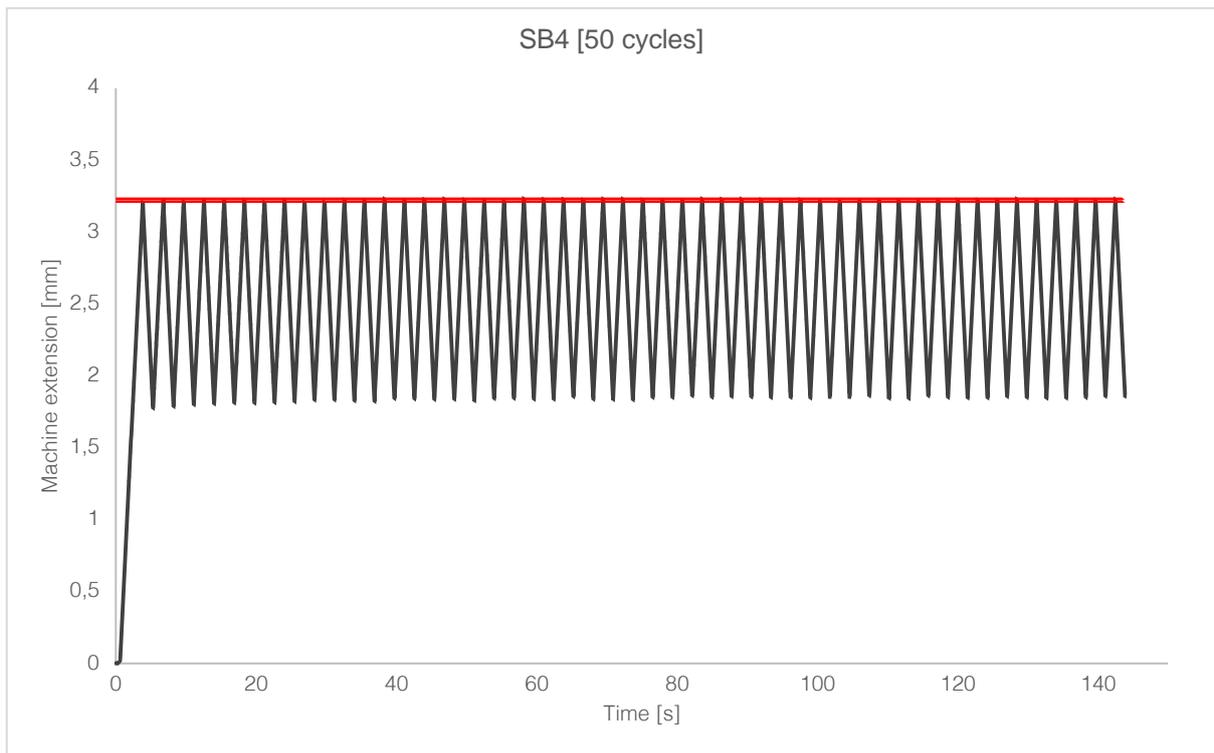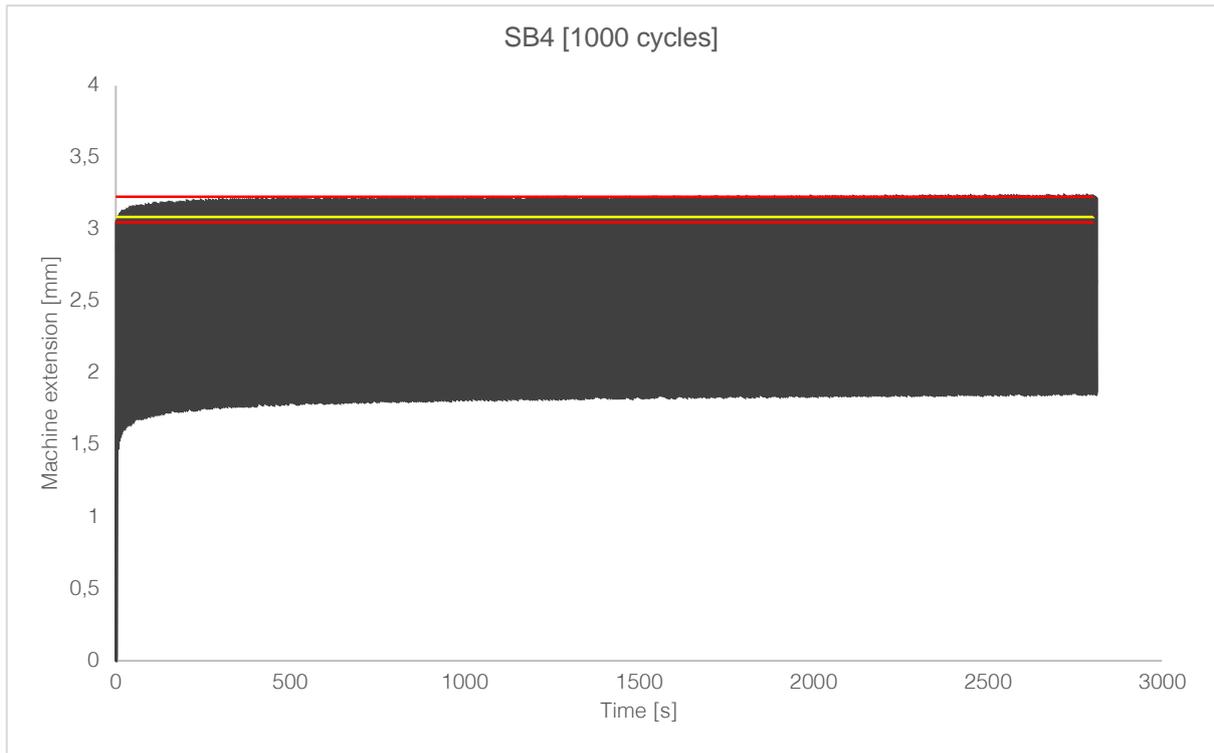
Figure A 10: Time-extension curves for the 1000 and 50 cycles test for SB4. The extension of the first compression is indicated by the lower red line, the second compression by the yellow line the last compression by the upper red line. For the second test of 50 cycles only the first and last compression are shown.
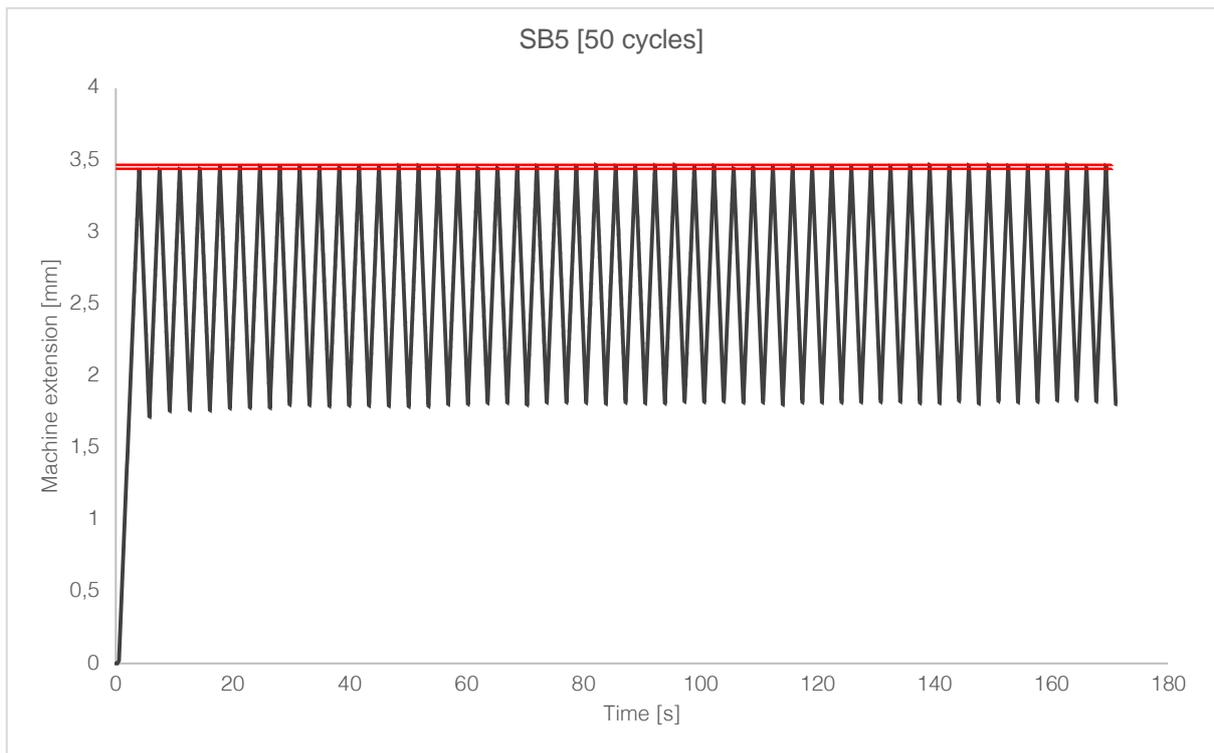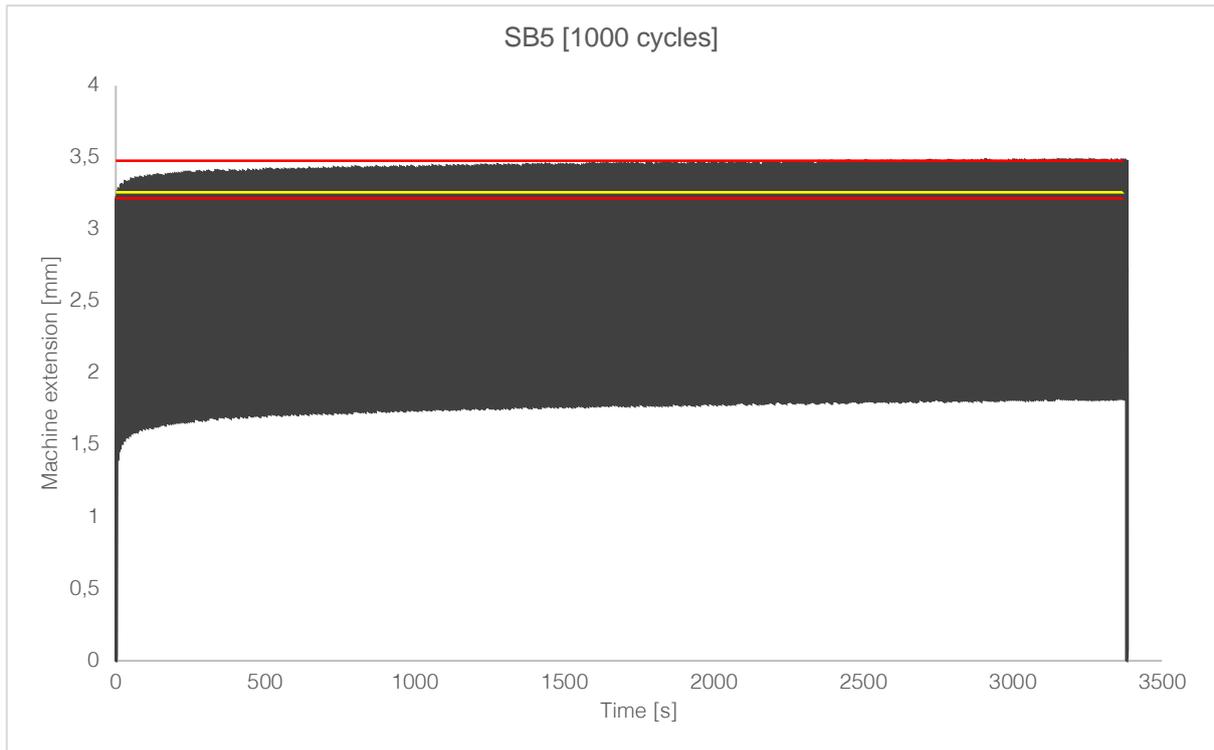
Figure A 11: Time-extension curves for the 1000 and 50 cycles test for SB5. The extension of the first compression is indicated by the lower red line, the second compression by the yellow line the last compression by the upper red line. For the second test of 50 cycles only the first and last compression are shown.